Hepatitis E Virus-induced antiviral response by plasmacytoid dendritic cells is modulated by the ORF2 protein

Garima Joshi[1§], Elodie Décembre[1], Jacques Brocard[2], Claire Montpellier[3], Martin Ferrié[3], Omran Allatif[1], Ann-Kathrin Mehnert[5], Johann Pons[6], Delphine Galiana[1], Viet Loan Dao Thi[5], Nolwenn Jouvenet[4], Laurence Cocquerel[3], and Marlène Dreux[1§].

Affiliations :

1: CIRI, Inserm, U1111, Université Claude Bernard Lyon 1, CNRS, UMR5308, École Normale Supérieure de Lyon, Univ Lyon, F-69007, Lyon, France

2: Université Claude Bernard Lyon 1, CNRS UAR3444, Inserm US8, ENS de Lyon, SFR Biosciences, Lyon 69007, France

3: Univ. Lille, CNRS, INSERM, CHU Lille, Institut Pasteur de Lille, U1019-UMR 9017-CIIL-Center for Infection and Immunity of Lille, F-59000 Lille, France.

4: Institut Pasteur, Université de Paris, CNRS UMR 3569, Virus sensing and signaling Unit, 75015 Paris, France

5: Department of Infectious Diseases, Virology, Heidelberg University, Medical Faculty Heidelberg, Heidelberg, Germany and German Centre for Infection Research (DZIF), Partner Site Heidelberg, Heidelberg, Germany

6: Sup'biotech : École Des Ingénieurs En Biotechnologies, Villejuif, Paris

§: To whom correspondence should be addressed: Dr. Marlène Dreux, CIRI, 50 Avenue Tony Garnier, 69007 Lyon, France. E-mail : marlene.dreux@ens-lyon.fr ; Garima Joshi, CIRI, 50 Avenue Tony Garnier, 69007 Lyon, France. E-mail: garima.joshi@ens-lyon.fr

Abstract

Type I and III interferons (IFN-I/III) are critical to protect the host during viral infection. IFN-mediated antiviral responses against hepatitis E virus (HEV) are suppressed and defeated by viral escape mechanisms at play in infected hepatocytes. Here, we studied the anti-HEV function of IFN secreted by plasmacytoid dendritic cells (pDCs), which are specialized producers of IFNs. We showed that pDCs co-cultured with HEV-infected cells secreted IFN in a cell-to-cell contact-dependent manner. Pharmacological inhibitor and antibodies targeting contact proteins revealed that pDC response against HEV required the endosomal nucleic-acid sensor TLR7 and adhesion molecules, such as ICAM-I and $\alpha_L\beta_2$-integrin. IFNs secreted by pDCs reduced viral spread. Intriguingly, ORF2, the capsid protein of HEV, can be produced in various forms by the infected cells. During infection, a fraction of the intracellular ORF2 protein localizes into the nucleus while another ORF2 fraction packages viral genomes to produce infectious virions. In parallel, glycosylated forms of ORF2 are also massively secreted by infected cells. Using viral genome expressing ORF2 mutants, we showed that glycosylated ORF2 forms contribute to better recognition of infected cells by pDCs by regulating contacts between infected cells and pDCs. ORF2 forms may thus modulate pDC-mediated anti-HEV response. Together, our results suggest that liver-resident pDCs, which exhibit comparable IFN-producing ability as blood-derived pDCs, may be essential to control HEV replication.

Introduction

Hepatitis E virus (HEV) is the most common cause of acute viral hepatitis worldwide. It has been estimated that this virus infects approximately 100 million people every year and is responsible for 14 million symptomatic cases and 300,000 deaths, mainly in regions of the world with poor sanitary conditions **(Li et al., 2020)**. Although HEV infection is usually asymptomatic and self-resolving, severe forms or chronic infections have been described, mainly in pregnant women and immunocompromised patients, respectively **(Lhomme et al., 2020)**. This underscores the significance of host immunity as a crucial factor influencing the outcome of the disease. In addition, HEV infection is associated with a broad range of extrahepatic manifestations, including renal and neurological disorders **(Songtanin et al., 2023)**. The *Orthohepevirus A* species of the *Orthohepevirus* genus contains five HEV genotypes (gt) that are pathogenic in humans. HEV gt1 and gt2 are primarily transmitted through soiled water, exclusively infect humans, and are responsible for waterborne hepatitis outbreaks in developing countries. In contrast, industrialized countries usually fall victim to HEV gt3 and gt4, which have a zoonotic origin **(Doceul et al., 2016)**. Chronic human infection with camel-associated HEV gt7 has also been reported **(Lee et al., 2016)**. Alarmingly, a rat HEV from the *Orthohepevirus C* species, exhibiting a potential to cause severe acute hepatitis in even immunocompetent individuals, was recently reported to be transmitted to humans **(Andonov et al., 2019; Sridhar et al., 2018)**.

The most common genotype causing chronic HEV infection in the developed world is gt3 **(Z. Ma et al., 2022)**. The evolution of HEV infection towards chronicity in immunocompromised gt3-infected patients, the transmission of HEV through blood transfusion, a growing number of diagnosed HEV cases, and complications in patients with pre-existing liver disease collectively contribute to the recognition of HEV infection as a burgeoning issue in industrialized countries **(Sayed et al., 2017)**. Importantly, HEV was recently ranked 6th among the top 10 zoonotic viruses presenting the greatest risk of spillover and spread to humans **(Grange et al., 2021)**.

HEV has a single-stranded, positive-sense RNA genome that contains three open reading frames (ORFs): ORF1, ORF2 and ORF3 **(Tam et al., 1991)**. ORF1 encodes the non-structural ORF1 polyprotein that displays domains essential for viral replication including the RNA-dependent RNA-polymerase (RdRp) **(Koonin et al., 1992)**. The RdRp produces a negative-

sense RNA replicative intermediate, which serves as a template for the subgenomic RNA. The subgenomic RNA encodes both ORF2 and ORF3 proteins **(Graff et al., 2006)**. ORF2 protein is the viral capsid protein and ORF3 is a small multifunctional phosphoprotein, involved in particle egress **(Nimgaonkar et al., 2018)**.

ORF2, which is composed of 660 amino acids, is produced in 3 forms: infectious ORF2 (ORF2i), glycosylated ORF2 (ORF2g), and cleaved ORF2 (ORF2c) **(Montpellier et al., 2018)**. The precise sequences of ORF2i, ORF2g and ORF2c proteins have been proposed by two groups **(Ankavay et al., 2019; Hervouet et al., 2022; Montpellier et al., 2018; Yin et al., 2018)**. The ORF2i protein is not glycosylated and forms the structural component of infectious particles. In contrast, ORF2g and ORF2c proteins (herein referred to as ORF2g/c) are highly glycosylated, secreted in large amounts in the culture supernatant (*i.e.,* about 1000x more than ORF2i) and are the most abundant ORF2 forms detected in patient sera, likely targeted by patient antibodies **(Ankavay et al., 2019; Montpellier et al., 2018)**. Thus, ORF2g/c forms may act as a humoral decoy that inhibits antibody-mediated neutralization due to their antigenic overlap with HEV virions **(Yin et al., 2018)**. Whether ORF2g/c proteins play a specific role in the HEV life cycle, and how ORF2 forms regulate the innate immune responses need to be elucidated. ORF2 forms are produced from different pathways, including a major one in which the ORF2 proteins are directed to the secretion pathway, where they undergo maturation, glycosylation, and are subsequently released in significant quantities. A fraction of cytosolic ORF2i proteins is delivered to the virion assembly sites **(Bentaleb et al., 2022; Hervouet et al., 2022)** while another fraction of ORF2i proteins translocate into the nucleus of infected cells, presumably to regulate host immune responses **(Ankavay et al., 2019; Hervouet et al., 2022; Lenggenhager et al., 2017)**.

Viral genomes can be recognized by cytosolic sensors *i.e.,* RIG-I, MDA5, LGP2 **(Rehwinkel & Gack, 2020)**, whose activation leads to the induction of type I and III interferons (IFN-I/III) pathways. HEV has developed many mechanisms to inhibit the IFN response *via* its three ORFs, described as follows. HEV gt1 ORF1 protein blocks RIG-I and Tank-binding kinase (TBK)-1 ubiquitination in hepatoma cells, thereby suppressing the pathway of IFN induction **(Nan et al., 2014)**. The amino-terminal region of HEV gt3 ORF1, harboring a putative methyltransferase (Met) and a papain-like cysteine protease (PCP) functional domain, inhibits IFN-stimulated response element (ISRE) promoter activation by inhibiting STAT1 nuclear translocation and phosphorylation **(Bagdassarian et al., 2018)**. Moreover, HEV gt1 and gt3

ORF2 protein antagonizes IFN induction in HEV-infected hepatocytes by inhibiting phosphorylation of the transcriptional regulator IRF3 **(Lin et al., 2019)**. The ORF3 protein of the HEV gt3 can also suppress IFN response by blocking STAT1 phosphorylation **(Dong et al., 2012)**.

In human hepatoma cells and primary hepatocytes, HEV infection induces only IFN-III production **(Wu et al., 2018; Yin et al., 2018)**, which is comparatively less potent at lower doses and early time points than IFN-I **(Lazear et al., 2019)**. However, elevated expression of IFN-stimulated genes (ISGs), which are effectors of IFN-I/III, was detected in the whole blood of HEV-infected patients **(Moal et al., 2013; Sayed et al., 2017; Yu et al., 2010)**, as well as in experimentally infected mice engrafted with human hepatocytes and chimpanzee **(Sayed et al., 2017; Yu et al., 2010)**. It must also be noted that the infectious HEV, with a complete replication cycle, has been shown to be more sensitive to IFNα treatment than the subgenomic replicon **(Zhou et al., 2016)**. Therefore, the host immune system can presumably mount an immune response to fight off HEV despite the attenuation of immune signaling within the host cells. Plasmacytoid dendritic cells (pDCs), which are key producers of IFN, could be instrumental in effectively counteracting the evasion strategies employed by HEV within the liver microenvironment. As pDCs are resistant to virtually all viruses **(Silvin et al., 2017),** these do not express viral proteins that may block IFN induction. pDCs are an immune cell type known to produce up to 1000-fold more IFNs than any other cell type **(Reizis, 2019)**. They are thus pivotal for host control of viral infections **(Venet et al., 2023; Yun et al., 2021; Reizis, 2019; Webster et al., 2016).** They also recruit NK cells at the site of viral replication, favor virus-specific T cell responses **(Cervantes-Barragan et al., 2012; Reizis, 2019; Swiecki et al., 2010; Webster et al., 2016, 2018)**, and secrete a large panel of pro-inflammatory cytokines, *e.g.,* tumour necrosis factor alpha (TNFα) and interleukin-6 (IL-6) **(Reizis, 2019)**. pDC stimulation is mediated by the recognition of viral nucleic acid by Toll-like receptors (TLR)-7 and -9, which localize in the endo-lysosomal compartment **(Reizis, 2019)**. In the case of RNA viruses, TLR7-ligand engagement results in the formation of a signal complex comprising IRAK1 (interleukin-1 receptor-associated kinase 1), IRAK4, and TRAF6 (tumor necrosis factor receptor–associated factor 6), in a MyD88-dependent (myeloid differentiation primary-response gene 88) manner. This further triggers the translocation of IRF7 (interferon-regulatory factor 7) into the nucleus, where it can induce the transcription of type I IFN genes. In addition, the NF-κB (nuclear factor-κB) and MAPKs (mitogen-activated protein kinases) mediated signaling are also activated **(Gilliet et al., 2008)**. It has been shown that liver pDCs retain the

ability to produce copious amounts of IFNα **(Doyle et al., 2019)**. Whether liver-resident pDCs contribute to the control of HEV replication is unknown. Here, by using hepatocyte-derived cell lines selected for their immunocompetence, we investigated the ability of HEV-infected cells to stimulate pDCs, and defined how ORF2 forms contribute to this process.

164 **Results**

165

166 **Immunocompetence of HEV cellular models**.

167 The magnitude of the type I and III interferons (herein referred to as IFN-I/III) responses
168 against viruses varies among cell types. We thus first assessed the immunological robustness
169 of three cell lines, namely Huh-7.5, HepG2/C3A and PLC3 cells, which are permissive to HEV
170 **(Montpellier et al., 2018; Schemmerer et al., 2016; Shukla et al., 2011)**. Huh 7.5 cells are a
171 subclone of the hepatoma Huh-7 cells that express an inactivate version of RIG-I and thus
172 display an increased permissiveness to viral infection **(Blight et al., 2002; Sumpter et al.,**
173 **2005)**. HepG2/C3A cells resemble liver parenchymal cells and were selected from the primary
174 hepatoblastoma derived cell line HepG2 for cell-contact inhibition, leading to a more
175 hepatocyte-like phenotype compared to the parental line **(Knowles et al., 1980)**. PLC3 cells
176 are a subclone of the PLC/PRF/5 hepatoma cell line broadly used to study HEV **(Montpellier**
177 **et al., 2018)**. We measured mRNA levels of two interferon-stimulated genes (*MXA* and *ISG15*)
178 and two cytokines (*TNFA* and *IL6*) in the three cell lines upon stimulation with polyI:C (**Fig.**
179 **1a-c**), which is a synthetic analog of dsRNA that activates TLR-3 when added to the cell
180 culture, and the cytosolic sensors RIG-I and MDA5 when transfected into cells. *MXA* and
181 *ISG15* are representatives of the IFN-I/III responses induced *via* IRF3-mediated signaling
182 while *TNFA* and *IL-6* are induced by NF-κB-signaling. All three cell types were deficient in
183 TLR3 activity as none of them responded to treatment with polyI:C (**Fig. 1a-c**). The expression
184 of *MXA*, *ISG15, TNFA* and *IL-6* remained unaffected upon polyI:C transfection in Huh-7.5
185 cells **(Fig. 1a)**. In contrast, the expression of these four genes was upregulated upon activation
186 of RIG-I and MDA5 in both HepG2/C3A and PLC3 cells **(Fig. 1b-c)**. Treatment with different
187 IFN types and TNFα has been shown to inhibit HEV replication to a certain extent **(Murata et**
188 **al., 2020; Todt et al., 2016; Wang et al., 2016; Zhou et al., 2016)**. Consequently, we
189 determined whether the three cell lines responded to stimulation by three recombinant
190 cytokines: IFN-β, IFN-λ3 *(i.e.,* representatives of Type I and III IFNs, respectively) or TNFα.
191 We found that IFN-β treatment induced the expression of *MXA* and *ISG15* in all three cell lines
192 but barely induced the proinflammatory cytokines, *TNFA* and *IL-6* **(Fig. 1a-c)**. The three cell
193 lines responded to the treatment with recombinant IFN-λ with an upregulation of *MXA* and
194 *ISG15* mRNA (**Fig. 1a-c**). However, only HepG2/C3A cells showed significant induction of
195 *IL-6* upon IFN-λ treatment **(Fig. 1b)**. Treatment with TNFα mainly upregulated the
196 proinflammatory cytokine *TNFA* in the three cell lines **(Fig. 1a-c)**. Together, our results show

197 that HepG2/C3A and PLC3 cells are sufficiently immunocompetent and were therefore
198 selected for further investigation.
199
200 Next, PLC3 and HepG2/C3A cells were electroporated with capped RNA of the HEV gt3 p6
201 strain **(Shukla et al., 2012)**. Immunostaining of ORF2 protein in PLC3 and HepG2/C3A cells
202 at 6 days post-electroporation (d.p.e.) confirmed viral replication **(Supplementary Fig. 1a)**. In
203 addition, we optimized a staining protocol to quantify ORF2-positive cells by flow cytometry.
204 Flow cytometry analyses showed that about 50% of PLC3 cells were positive for ORF2 at 6
205 d.p.e. **(Supplementary Fig. 1b)**. Consistently, RT-qPCR analyses showed that HepG2/C3A
206 and PLC3 cells produced a significant amount of viral RNA **(Fig. 1d-e)** compared to mock-
207 electroporated cells (Control). HepG2/C3A and PLC3 cells are thus suitable models to perform
208 immunological studies in the context of HEV replication.
209
210 **Activation of pDCs upon contact with HEV-infected cells leads to antiviral response**.
211 Next, we looked at expression levels of two ISGs and three cytokines in HEV-replicating PLC3
212 and HepG2/C3A cells (**Fig. 2a-b**). We found a modest increase of mRNA levels of the 5 tested
213 genes (*MXA*, *ISG15*, *TNFA*, *IL-6*, *IFN-λ1*) in HepG2/C3A cells at 6 d.p.e. **(Fig. 2a;** left panel**)**.
214 In PLC3 cells, mRNA abundance of *MXA*, *ISG15* and *IL-6* remained unchanged **(Fig. 2b;** left
215 panel**)**. These results are in accordance with the higher responsiveness of HepG2/C3A cells to
216 activation of cytosolic sensors and cytokines as compared to PLC3 cells **(Fig. 1b-c)**. The level
217 of *IFN-λ1* mRNA, which has known anti-viral role against HEV in mice **(Sari et al., 2021)**,
218 increased upon viral replication in both cell types **(Fig. 2a-b;** left panels**)**. In addition, *TNFA*
219 expression was slightly inhibited in HEV-replicating PLC3 cells **(Fig. 2b;** left panel**)** in
220 accordance with previous results **(Hervouet et al., 2022).** IL-6 was poorly induced in HEV-
221 replicating HepG2/C3A cells. These results showed that, although HepG2/C3A and PLC3 cells
222 are immunocompetent upon stimulation (**Fig. 1**), IFN-I/III response is only modestly induced
223 upon HEV replication in HepG2/C3A cells and marginally in PLC3 cells. In line with previous
224 *in vitro* studies **(Bagdassarian et al., 2018; Dong et al., 2012; Lin et al., 2019; Nan et al.,**
225 **2014)**, these results suggest that HEV is a poor inducer of IFN response.
226
227 *In vivo* studies of HEV infection (i.e., at tissue level) have, nonetheless, demonstrated induction
228 of antiviral responses **(Moal et al., 2013; Sayed et al., 2017; Yu et al., 2010)**. We thus thought
229 to investigate whether human primary pDCs can mount the IFN-I/III response. The human
230 primary pDCs were stimulated upon co-culture for 16 hours with HEV-replicating cells. As in

231 aforementioned experiments, we analyzed mRNA abundance of *MXA, ISG15, IFN- λ1*, *TNFA,*
232 *and IL-6* by RT-qPCR **(Fig. 2a-b;** right panels**)**. We observed non-significant upregulated
233 expression of all these effectors when pDCs were co-cultured with HEV-infected cell lines, as
234 compared to basal levels with uninfected cells (**Fig. 2a-b, right panels**). *IFN- λ1*, nevertheless,
235 was significantly upregulated when HEV-infected cells and pDCs were co-cultured. Overall,
236 likely due to the inhibitory mechanisms of HEV viral products in hepatocyte-derived cell lines
237 targeting IFN-I/III amplification pathways, there was a poor activation of downstream
238 effectors, ISGs and cytokines in the mixed cell culture, with the exception of *IFN- λ1*.
239
240 We thus tested whether pDCs can produce IFNs in response to HEV-infected cells by
241 quantifying the secreted levels of multiple subtypes of IFNα as representative of IFN-I
242 signaling **(Fig. 2c)**. HEV-replicating PLC3 cells did not produce detectable IFNα levels, in
243 accordance with previous findings showing that HEV replication does not induce IFN-I
244 secretion **(Moal et al., 2013; Nan et al., 2014; Sayed et al., 2017; Yu et al., 2010).** In contrast,
245 when pDCs were co-cultured with HEV-replicating PLC3 cells, more than 1000 pg/ml of IFNα
246 were secreted, whereas no IFNα was detected when pDCs were co-cultured with uninfected
247 control cells **(Fig. 2c)**. pDCs exposed to the filtered supernatant [SN] collected from HEV-
248 replicating cells secreted a small amount of IFNα **(Fig. 2c)**, suggesting that physical contact
249 between pDCs and HEV-replicating cells is required for the robust IFN-I secretion, a
250 characteristic of pDCs. Therefore, we assessed whether HEV-replicating PLC3 cells activated
251 pDCs when the two cell types were separated by a 0.4 µm-permeable membrane, which allows
252 diffusion of virions but not cells. In this Transwell setting, pDCs placed in the top chamber did
253 not produce any IFNα, validating that physical contact between the cells is required for pDC
254 stimulation **(Fig. 2d)**. Imiquimod [IMQ], which is a soluble agonist of TLR7 **(Gibson et al.,**
255 **2002)**, was used as an additional positive control to rule out non-specific effect of the setting
256 **(Fig. 2d)**. Furthermore, when the co-cultures were treated with blocking antibodies against
257 ICAM-I and $\alpha_L\beta_2$-integrin, two cell-cell adhesion proteins that mediate cellular contacts **(Assil,**
258 **Coléon, et al., 2019; Marlin & Springer, 1987)**, pDC response to infected cells was
259 significantly reduced as compared to untreated pDCs in co-culture with HEV-replicating cells
260 **(Fig. 2e)**. Since TLR7 is responsible for sensing replicative viral RNAs in pDCs **(Assil,**
261 **Coléon, et al., 2019; Reizis, 2019; Webster et al., 2016)**, we tested its contribution in pDC
262 response to HEV-replicating cells. When the co-cultures were treated with the TLR7 inhibitor
263 IRSS661, no IFNα was secreted (**Fig. 2e**), suggesting that stimulation of pDCs by HEV-
264 replicating cells is mainly mediated by TLR7. Together, our results show that direct contacts

265 mediated by ICAM-I and, at least in part, with $\alpha_L\beta_2$-integrin, enable pDCs to sense and respond
266 to HEV-replicating cells in a TLR7-dependent manner.
267
268 We then tested whether IFNα produced by pDCs inhibited viral propagation in either
269 HepG2/C3A or PLC3 cells **(Fig. 2f-h)**. Upon 18 hours of co-culture of pDCs with HepG2/C3A
270 electroporated with HEV RNA **(Fig. 2f)**, we observed a 1-log decrease in viral RNA yield
271 (readout for viral replication) compared with the absence of pDCs. At this early time point of
272 co-culture, the impact of pDCs on viral RNA replication was not yet observed for PLC3 cells
273 **(Fig. 2g)**. Thus, we study the effect of pDCs on viral production in HEV-replicating PLC3 cells
274 when co-cultured with pDCs for a longer period, *i.e.,* 48h. The disparity among results in the
275 two cell lines may be attributed to the lack of initial upregulation of ISGs in HEV-replicating
276 PLC3 cells, leading to an overall lowering of effect on viral replication than observed for
277 HepG2/C3A cells. Upon a longer co-culture of 48 hours with pDCs, we observed a 50%
278 reduction of HEV-infected cells as compared to cultures without pDCs **(Fig. 2h).**
279
280 To further examine whether pDC-mediated IFN response decreases the percentage of newly
281 infected cells, we co-cultured pDCs for 48 hours with a mixture of PLC3 cells, either
282 electroporated with HEV RNA and not expressing GFP ($ORF2^+/GFP^-$ cells) or uninfected cells
283 positive for GFP ($ORF2^-/GFP^+$). The impact of pDC response on HEV spread was assessed by
284 flow cytometry to quantify the percentage of newly infected cells ($ORF2^+/GFP^+$) in the
285 presence *versus* absence of pDCs (**Fig. 2i-j**). The results demonstrated that pDC response
286 reduced viral replication in cells replicating HEV prior to co-culture with pDCs **(Fig. 2j,** blue
287 bars**)** as well as controlled viral spread to naive GFP^+ cells by half, upon prolonged co-culture
288 **(Fig. 2j,** green bars**)**. Collectively, our results showed an effective control of HEV spread by
289 pDC-mediated antiviral activities involving IFN-I production, and the resultant cumulative
290 effect of upregulated ISGs.
291
292 **Modulation of pDC response by HEV expressing ORF2 mutant is dependent on the host**
293 **cell type**
294 pDCs responded to contact with HEV-infected cells *via* TLR7 recognition (**Fig. 2e**), suggesting
295 that HEV genome is transferred from infected cells to the endosomal compartments of pDCs,
296 where TLR7 localizes **(Dreux et al., 2012)**. The distinctive feature of the HEV ORF2 capsid
297 protein is its generation in three distinct forms (ORF2i, ORF2g, and ORF2c), each with
298 different localization and trafficking patterns within infected cells **(Ankavay et al., 2019;**

299 **Hervouet et al., 2022; Lenggenhager et al., 2017)**. To address whether these distinct ORF2
300 forms impact the host responses in infected cells, and consequently and/or additionally the
301 detection of infected cells by pDCs, we tested a series of ORF2 protein mutants of the p6 HEV
302 strain (WT) **(Supplementary Fig. 1c)**. The first mutant, called 5R/5A mutant, expresses an
303 ORF2 in which the arginine-rich motif (ARM) located in the ORF2 N-terminal region, serving
304 as a nuclear localization signal, was mutated and thus prevents ORF2 translocation into the
305 nucleus **(Hervouet et al., 2022)**. The NES mutant expresses an ORF2 that lacks one of its
306 nuclear export signals (NES), leading to its retention in the nucleus **(Hervouet et al., 2022)**.
307 Glycosylated proteins can influence immunological functions *via* their recognition by C-type
308 Lectin receptor (CLRs) **(Cambi et al., 2005)**, either by weakening TLR7 and TLR9-mediated
309 IFN-I/III response **(Florentin et al., 2012; Meyer-Wentrup et al., 2008)**, or contributing to
310 cell interaction and viral uptake **(Bermejo-Jambrina et al., 2018)**. Therefore, we generated an
311 additional mutant, called STOP mutant, expressing an ORF2 protein with a non-functional
312 signal peptide, preventing its translocation into the endoplasmic reticulum and thus production
313 of glycosylated ORF2g/c forms, as recently described **(Nagashima et al., 2023)**. This mutant
314 carries a stop codon in the ORF2 signal peptide, which does not affect ORF3 expression. In the
315 STOP mutant, ORF2 protein translation starts at the first initiation codon (Met^{1}), stops at stop
316 codon ($*^{10}$) and restarts at the second initiation codon (Met^{16}) (**Supplementary Fig. 2a**). PLC3
317 cells expressing this mutant produce intracellular ORF2i form (**Supplementary Fig. 2b,** right
318 panel), efficiently replicate HEV genome, (**Supplementary Fig. 2d**) and produce HEV
319 particles (**Supplementary Fig. 2c**, IP P1H1 and **Supplementary Fig. 2e-f**), but no ORF2g/c
320 proteins (**Supplementary Fig. 2c**, IP P3H2). Finally, a previously characterized replication-
321 defective p6 mutant (GAD) was also included in the analysis **(Emerson et al., 2013)**.
322
323 The subcellular distribution of ORF2 mutants, compared with wild-type (WT) ORF2, was first
324 characterized using confocal microscopic analyses. The WT ORF2 was found in both
325 cytoplasm and nucleus, in both HepG2/C3A and PLC3 cells **(Fig. 3a-b).** The 5R/5A mutant
326 was excluded from the nucleus whereas the NES mutant accumulated in the nucleus in both
327 cell types (**Fig. 3a-b**), in accordance with previous observations **(Ankavay et al., 2019;**
328 **Hervouet et al., 2022)**. The STOP mutant exhibited a localization similar to that of WT ORF2
329 (**Fig. 3a-b**). As expected, the GAD mutant, in which the polymerase active site was mutated
330 and thus is replication-defective, did not produce ORF2 (**Fig. 3a-b**). We then assessed viral
331 RNA yield produced in cells electroporated with the four mutant genomes or with WT genome
332 using RT-qPCR analysis, in order to attest comparable levels of HEV RNA, as a prerequisite

333 for testing the impact of this mutant panel on the response of co-cultured pDC. The HEV RNA
334 levels were similar across the mutants and WT genomes at 6 d.p.e. in the HepG2/C3A cells
335 **(Fig. 3c)**. PLC3 cells electroporated for 6 days with the WT, 5R/5A, NES and STOP mutant
336 genomes also yielded similar levels of viral RNAs (**Fig. 3d)**. About two-log less viral RNA
337 was recovered in HepG2/C3A and PLC3 cells expressing the GAD genome mutant **(Fig. 3c-**
338 **d).** Viral RNA detected in these cells likely represent 'input' RNA, i.e., electroporated viral
339 RNA.
340
341 Quantification of IFNα production by pDCs co-cultured with HepG2/C3A expressing the
342 different mutants demonstrated significant differences. First, pDCs co-cultured with
343 HepG2/C3A cells expressing the GAD mutant did not trigger a pDC response **(Fig. 3e)**, nor in
344 the context of PLC3 cells **(Fig. 3f)**. Albeit HEV RNA levels were reduced for GAD mutant, it
345 is tempting to hypothesize that active viral replication is required for mounting a pDC-mediated
346 viral response. Next, pDCs co-cultured with HepG2/C3A expressing 5R/5A demonstrated a
347 significant reduction of IFNα production as compared to WT and 5R/5A versus NES **(Fig. 3e)**.
348 These results suggested that, in this cellular model, the nuclear localization of ORF2 influences
349 pDC stimulation. pDC-mediated IFNα response was completely abolished upon co-culture
350 with PLC3 cells expressing the 5R/5A mutant **(Fig. 3f)**. Since comparable HEV RNA levels
351 were quantified in NES versus 5R/5A mutant **(Fig. 3d)**, ORF2 subcellular distribution, notably
352 its nuclear localization, which is abrogated for the 5R/5A mutant, may affect pDC response
353 against HEV. Since the 5R/5A mutant does not produce infectious viruses **(Hervouet et al.,**
354 **2022)**, pDC response against HEV might be modulated by viral particles release and/or nuclear
355 ORF2.
356
357 IFNα production was lower when pDCs were co-cultured with PLC3 cells expressing the STOP
358 mutant, as compared to cells expressing WT ORF2, suggesting that ORF2g/c forms contribute
359 to the pDC IFN-I response in these cells. The ORF2g/c produced by the WT ORF2 may be
360 recognized by the CLRs of pDCs, contributing to an enhanced response to immuno-stimulatory
361 RNA. Alternatively, ORF2g/c expression may facilitate viral RNA transfer to pDC and its
362 subsequent recognition by TLR7 in endosomes. However, the decrease of pDC response to the
363 STOP mutant was not observed for HepG2/C3A cells **(Fig. 3e)**.
364
365 Overall, the absence of pDC response to 5R/5A in PLC3 could, directly or indirectly, result
366 from ORF2-regulated functions, especially ORF2 nuclear translocation and/or production of

367 ORF2i. Taken together, our results show that ORF2 protein expression and localization in
368 producer cells modulate pDC response, at levels depending on the cellular context.
369
370 **Glycosylated ORF2 proteins contribute to contact between replicating cells and pDCs**
371
372 We sought to determine whether HEV ORF2-mediated regulation of the strength and duration
373 of cell-to-cell contacts could impact pDC response to infected cells. To achieve this, we
374 developed a confocal imaging pipeline that quantifies cell proximity between pDCs and
375 infected cells **(Supplementary Fig. 3a)**. Since more contrasting effects among ORF2 mutants
376 were observed in PLC3 cells than in HepG2/C3A cells **(Fig. 3)**, we selected PLC3 cells for
377 investigating the role of cell-to-cell contacts in pDC-mediated response.The pDCs and HEV-
378 infected cells were stained using CellTrace Violet (CTV) and CellTracker Red (CMPTX),
379 respectively, and then co-cultured and fixed after 4 hours **(Fig. 4a)**. HEV-infected cells were
380 identified using the P3H2 anti-ORF2 antibody, which recognizes all forms of ORF2
381 (ORF2g/c/i) **(Bentaleb et al., 2022)**. The raw images were analyzed by an ImageJ macro-
382 driven automatic analysis of cell-cell contacts. The two criteria for selection of contacts
383 between pDCs and infected cells were the distance between the two cell types (1µm) and a
384 contact area (>0µm^2) between the surfaces of the two cell types **(Supplementary Fig. 3b)**.
385
386 The percentage of ORF2 positive cells was within a comparable range among WT and the
387 mutants in PLC3 cells **(Fig. 4b)**, in agreement with their similar RNA levels **(Fig. 3d)**. As
388 compared to co-culture of pDCs with cells expressing WT ORF2, fewer cell-to-cell contacts
389 **(Fig. 4c)** between pDCs and cells expressing the 5R/5A were observed (*i.e.*, reproducible but
390 not significant) and a significant 40% decline in pDC contacts with cells expressing the STOP
391 mutant. Taking into consideration that the STOP mutant displayed a reduced induction of pDC
392 response (**Fig. 3f)**, this decline in pDC response to the STOP mutant could be due to reduced
393 cell-to-cell contacts. Nevertheless, no difference was observed in the quality or strength of
394 contacts, expressed in terms of contact area, across the mutants and WT **(Supplementary Fig.
395 3c)**. This indicates that pDC function is likely influenced by frequency of contact formation
396 rather than the area of contact between the infected cell and pDC, which was found to be
397 consistent across the wild-type and mutants. Together, our results suggest that ORF2g/c
398 production, and not nuclear ORF2, likely modulate the number of cell-cell contact and,
399 subsequently, pDC-mediated IFN-I response.
400

401 **DISCUSSION**

402

403 Several studies have highlighted the suppressive impact of HEV on IFN response **(Devhare et**
404 **al., 2021)**. Here, we investigated whether these inhibitory mechanisms can be overcome by
405 pDCs, which act as immune sentinels against viral infections. Given the limited number of
406 studies on cellular systems that effectively replicate HEV, we first determined the ability of
407 three hepatoma cell lines to respond to several immune stimuli and replicate the viral genome.
408 Based on their robust response to stimuli and their ability to replicate gt3 p6 strain HEV RNA,
409 we selected PLC3 and HepG2/C3A cells for further analyses. Upon 6 days of HEV RNA
410 electroporation, we observed a modest upregulation of IRF3 and NF-KB-mediated gene
411 expression in HepG2/C3A cells. *IFN-λ1* expression was upregulated in both cell types, in
412 agreement with studies recognizing type III IFN response as a fundamental anti-HEV cytokine
413 in hepatocytes both clinically **(Murata et al., 2020)** and *in vitro* **(Wu et al., 2018; Yin et al.,**
414 **2017)**. Even though HEV can persist in the presence of a sustained type III IFN response **(Yin**
415 **et al., 2017)**, this response prevents inflammation and helps maintain barrier integrity **(Broggi**
416 **et al., 2020)**. Importantly, *TNFA* upregulation was reduced by HEV in PLC3 cells, in
417 agreement with previous data obtained in PLC3 cells **(Hervouet et al., 2022)**. This was not
418 observed for HepG2/C3A cells, suggesting that HEV modulates NF-KB-mediated signaling in
419 a cell-type specific manner. While exhibiting strong anti-viral effects **(Wang et al., 2016)**,
420 TNFα is also implicated in pro-inflammatory processes exacerbating the severity of liver
421 disease upon HEV infection **(Behrendt et al., 2017)**. Importantly, the differences in immune
422 profiles of PLC3 cells and HepG2/C3A may be due to the expression of Hepatitis B surface
423 antigen (HBsAg) by PLC3 cells, a known limitation of this cell type **(MacNab et al., 1976)**.
424 Nevertheless, these cells may relevantly mimic the immune characteristics of individuals with
425 pre-existing or previous infections or medical condition, predisposing them to HEV infection.
426 Notably, HEV replicating cells alone secreted no detectable IFNα, in accordance with previous
427 studies using HepG2 cells **(Yin et al., 2017)** and iPSC-HLCs **(Wu et al., 2018)**.

428

429 Upon co-culture of hepatoma cells with pDCs, *IFN-λ1* was significantly up-regulated. IFN-λ1
430 expression by pDCs has been documented to actively participate in pDC response *e.g.*, against
431 human cytomegalovirus and SARS-CoV-2 **(Venet et al., 2023; Yun et al., 2021)**. Whether the
432 source of *IFN-λ1* upregulation were HEV- replicating cells, pDCs, or both cell types in concert,
433 remains to be determined. The expression of ISGs barely increased at 18h post co-culture,
434 opening the possibility of ISG upregulation upon prolonged co-culture. Since the expression

435 of these effectors is crucial for restricting viral replication **(Schneider et al., 2014)**, this
436 represents a possible Achilles' heel in host immune defense against HEV as this might
437 contribute to HEV persistence in culture and its elimination might be challenging even after
438 prolonged exposure to high doses of IFNs **(Todt et al., 2016)**. This assumption is in agreement
439 with the decrease of viral spread propagation/replication that we reported at a late time point
440 of coculture. This makes the primary IFN response by pDCs crucial to induce ISGs, even if
441 prolonged exposure to IFNs may be necessary. The lack of ISG expression was overcome by
442 pDCs against HEV in the form of a strong IFN-I response when co-cultured with infected cells,
443 known to activate ISG expression in neighboring cells **(Bourdon et al., 2020)** and also to
444 facilitate adaptive immune responses **(Crouse et al., 2015)**. Along the same line, the IFN-I
445 response against HEV was dependent on pDC-infected cell contact formation. This was
446 orchestrated by ICAMI and $\alpha_L\beta_2$-integrin and TLR7, in agreement with results obtained for
447 other viral infection **(Yin et al., 2017)**. The contact between pDCs and infected cells is
448 beneficial for host defense, considering that HEV is resistant to exogenous IFN treatment **(Todt
449 et al., 2016; Wang et al., 2016)**. On a different note, a prior study has shown that HEV-ORF3
450 can attenuate TLR7 expression **(Lei et al., 2018)**, this effect is less likely to be observed for
451 pDCs as these are non-permissive to most viruses **(Reizis, 2019; Silvin et al., 2017; Venet et
452 al., 2023)**. pDC response failed to control HEV replication after 18h of co-culture with PLC3
453 cells but effectively controlled HEV replication in HepG2/C3A under the same conditions.
454 This difference between cell lines to restrict viral replication may be attributed to intrinsic
455 immune signaling, which is more robust for the HepG2/C3A cells than for PLC3 cells. Upon
456 further scrutiny, pDC-mediated IFN response reduced HEV production by 50% 48h post co-
457 culture in PLC3 cells. This also contributed to an overall decline in viral spread to neighboring
458 cells. These results confirmed the need for a prolonged IFN response for controlling HEV
459 replication.
460
461 In the absence of ORF2 nuclear translocation (5R/5A mutant), pDC IFN-I response was
462 diminished in HepG2/C3A cells and abolished in PLC3 cells. Furthermore, when ORF2
463 accumulated in the nucleus (NES mutant), there was no difference in pDC response as
464 compared to the wild-type. Additionally, the depletion of ORF2g/c secretion (STOP mutant)
465 lowered the pDC response in PLC3 cells but not in HepG2/C3A cells. Altogether, these
466 observations suggest that ORF2 nuclear translocation and secretion of glycosylated ORF2g/c
467 forms might modulate pDC response in a cell-type dependent manner. Since many adhesion
468 molecules are ISGs **(N. Ma et al., 2022; Parr & Parr, 2000)** and can impact the ability of

469 HEV-mutant harboring cells to form cell-to-cell contact, we compared their pDC contact-
470 forming propensity. Only cells harboring the STOP mutant differed from wild-type HEV cells
471 in their ability to form contacts with pDCs. These results support the hypothesis of a decreased
472 attraction of pDCs towards STOP-expressing cells due to the absence of ORF2g/c secretion.
473 We should also take into account the decrease in viral infectivity in the absence of ORF2g/c
474 **(Supplementary Fig. 2e)**, which could in turn lead to reduced pDC IFN response. Even though
475 incubation with purified ORF2g/c does not impact HEV entry **(Yin et al., 2018)**, our results do
476 raise further questions on whether its secretion can indirectly offer an advantage to HEV for
477 spreading to the neighboring cell by improving cell-cell adhesion, a relatively easier route of
478 viral transmission **(Zhong et al., 2013)**. Many studies have demonstrated that glycosylation is
479 a common factor affecting cell-cell adhesion **(Gu et al., 2012; Ohtsubo & Marth, 2006)**.
480 When rhesus macaques were infected with HEV variant that did not express ORF2g/c or
481 ORF2s, viral replication was attenuated and viral shedding in feces declined significantly as
482 compared to infection with WT HEV **(Ralfs et al., 2023)**. Therefore, ORF2 g/c may not be
483 essential for viral replication but it may be instrumental for efficient viral production.
484
485 Our findings emphasize the significance of the ongoing co-evolution between hosts and
486 pathogens, allowing the virus to disseminate while concurrently enhancing its detection by
487 immune cells. The difference in pDC response among HEV WT, NES *versus* 5R/5A still
488 remains enigmatic but it paves a direction for further exploration in this exciting field. In the
489 case of 5R/5A PLC3 cells, a probable explanation for the absence of pDC response could be
490 the lack of infectious ORF2 (ORF2i) **(Hervouet et al., 2022)**. On the other hand, the presence
491 of pDC response to 5R/5A HepG2/C3A cells may also imply regulation of pDC response at an
492 additional level, *i.e.*, cell-type dependent regulation. Since pDCs mounted an IFN-I response
493 against 5R/5A in HepG2/C3A cells, we propose that this detection could have been fueled by
494 a successful upregulation of ISGs within HepG2/C3A cells compared to PLC3 cells upon HEV
495 infection. Importantly, TNF signaling is induced in HepG2/C3A cells and inhibited in PLC3
496 cells. Since TNF signaling regulates cell adhesion via ICAM-1 **(Reglero-Real et al., 2014)** and
497 activates an autocrine loop with low and sustained production of type I IFNs **(Yarilina et al.,
498 2008)**, it could contribute to differential pDC response for the two cell-types. Globally, the
499 HEV mutants advanced our comprehension about viral regulation of the IFN response and also
500 mechanistic nuances of viral recognition by pDCs. In summary, our findings suggest that pDC
501 response is likely regulated by (i) transfer of viral entities to pDCs for recognition (ii) number
502 of cell-to-cell contacts, and (iii) intrinsic immune state of the infected cells.

503 **Material and Methods**
504
505 **Reagents and antibodies**

506 Reagents used for pDC isolation are: Ficoll-Hypaque (GE Healthcare Life Sciences), BDCA-
507 4-magnetic beads (MACS Miltenyi Biotec), LS Columns (MACS Miltenyi Biotec) and bottle
508 top vacuum filters 0.22 µm (Nalgene). Other reagents included Poly(I:C) (LMW, Invivogen)
509 as TLR3 agonist, Imiquimod as TLR7 agonist (Invivogen), and TLR7 antagonist (IRS661, 5'-
510 TGCTTGCAAGCTTGCAAGCA-3' synthesized on a phosphorothionate backbone MWG
511 Biotech). The following antibodies were used: mouse anti-α_L integrin (clone 38; Antibodies
512 Online); mouse anti-ICAM-1 (Clone LB-2 ; BD Bioscience); mouse anti-HEV ORF2 1E6,
513 (Millipore, antibody registry #AB-827236), mouse anti-ORF2i/g/c P3H2 **(Bentaleb et al.,**
514 **2022)** and mouse anti-ORF2i P1H1 **(Bentaleb et al., 2022)**. Goat anti-Mouse IgG2b Cross-
515 Adsorbed Secondary Antibody Alexa Fluor 488 (Thermo Fisher Scientific Catalog #A-21141)
516 were used for flow cytometry analysis.

517 **Cell Lines**

518 PLC3 cells, a subclone of PLC3/PRF/5 cells **(Montpellier et al., 2018)**, Huh-7.5 cells
519 (RRID:CVCL_7927) are hepatoma cells derived from Huh-7 cells **(Blight et al., 2002)**, and
520 HepG2/C3A cells (ATCC CRL-3581) (provided by Dr. V.L. Dao Thi and Dr. D. Moradpour)
521 were used. PLC3 and Huh-7.5 cells were maintained in Dulbecco's modified Eagle medium
522 (DMEM) supplemented with 10% FBS, 100 units (U)/ml penicillin, 100 mg/ml streptomycin,
523 2 mM L-glutamine and non-essential amino acids, 1 mM sodium pyruvate (Life Technologies)
524 at 37°C/5% CO_2. HepG2/C3A were maintained in DMEM (Glutamax, Pyr-) supplemented
525 with 10% FBS, 100 units (U)/ml penicillin at 37°C/5% CO_2.

526 **pDC isolation and culture**

527 pDCs were isolated from blood from healthy adult human volunteers which was obtained from
528 the '*Etablissement Francais du Sang'* (EFS; Auvergne Rhone Alpes, France) under the
529 convention EFS 16–2066 and according to procedures approved by the EFS committee.
530 Informed consent was obtained from all subjects in accordance with the Declaration of
531 Helsinki. Information on sex and age was available for all subjects, yet we previously showed
532 that pDC responses are within the same range for all donors **(Decembre et al., 2014)**. PBMCs
533 were isolated using Ficoll-Hypaque density centrifugation and pDCs were positively selected
534 from PBMCs using BDCA-4-magnetic beads (MACS Miltenyi Biotec), as previously

535 described **(Decembre et al., 2014; Dreux et al., 2012; Venet et al., 2023)**. The typical yields
536 of PBMCs and pDCs were 500-800x10^6 and 1-2x10^6 cells, respectively, with a typical purity
537 of >95% pDCs. Isolated pDCs were maintained in RPMI 1640 medium (Life Technologies)
538 supplemented with 10% FBS, 10 mM HEPES, 100 units/ml penicillin, 100 mg/ml
539 streptomycin, 2 mM L-glutamine, non-essential amino acids and 1 mM sodium pyruvate at
540 37°C/5% CO_2.

541 **Stimulation of cells for immune response using agonists and recombinant cytokines.**

542 PLC3 cells were seeded in 24-well plates at a concentration of 8.10^4 cells/well. After 24h, cells
543 were incubated with poly(I:C) LMW in complete medium at a concentration of 25 µg/ml and
544 100 µg/ml, in a total volume of 0.5ml medium. Alternatively, cells were transfected with
545 poly(I:C) LMW at a concentration of 0.3 µg/ml and 2 µg/ml. Lipofectamine 2000 (Invitrogen)
546 in Opti-MEM I reduced serum media was used for transfection according to the manufacturer's
547 protocol. IFN-β subtype 1a (Invitrogen, Catalog#PHC4244), IFN-λ3/Interleukin-28B (IL-28B)
548 (PBL Interferon Source #11820-1), TNF (Cell Signalling Technology #16769) were added at
549 a concentration of 100U/ml, 100ng/mL and 535 U/mL, respectively, in a total volume of 0.5
550 mL medium per well. The cells were harvested 6h post-treatment for RNA extraction.

551 **Analysis of transcriptional levels by RT-qPCR.**

552 RNAs were isolated from cells harvested in guanidinium thiocyanate citrate buffer (GTC) by
553 phenol/chloroform extraction procedure, as described previously (Assil, Coléon, et al., 2019).
554 The mRNA levels of human *MXA, ISG15*, *IFN-λ1, IL6, TNFA, ORF2* and glyceraldehyde-3-
555 phosphate dehydrogenase (*GADPH*) were determined by RT-qPCR using High-Capacity
556 cDNA Reverse Transcription Kit (ref# 4368813) and PowerUp™ SYBR™ Green Master Mix
557 (ref# A25778) for qPCR run on QuantStudio6 PCR system and analyzed using QuantStudio
558 Design and Analysis Software (Thermo Fisher Scientific). The mRNA levels were normalized
559 to *GADPH* mRNA levels. The sequences of the primers used for RT-qPCR are as listed in
560 **supplementary Table 1**.

561 **Plasmids and electroporation for HEV infectious system.**

562 The plasmid pBlueScript SK(+) carrying the DNA of the full length genome of adapted gt3
563 Kernow C-1 p6 strain, (GenBank accession number JQ679013, kindly provided by Dr S.U.
564 Emerson), was used as the wild-type genome. The 5R/5A and NES mutant plasmids were

565 previously described **(Hervouet et al., 2022)**. The STOP mutant was generated by site directed
566 mutagenesis using the following primers :

567 P6/mutstop-F : TGTTCTGCTGCTGTagTTCGTGTTTCTGCCTATGC

568 P6/mutstop-R : GGCAGAAACACGAActACAGCAGCAGAACAACCC

569 The Stop mutation was introduced by sequential PCR steps, as previously described **(Ankavay**
570 **et al., 2019)**, and verified by DNA sequencing. The non-replicative GAD mutant plasmid was
571 a gift from Dr V. L. Dao Thi **(Emerson et al., 2013)**. To prepare genomic HEV RNAs (capped
572 RNA), the wild type and mutant pBlueScript SK(+) HEV plasmids were linearized at their 3′
573 end with the MluI restriction enzyme (NEB) and transcribed with the mMESSAGE
574 mMACHINE T7 Transcription kit (Ambion #1344). 10 µg capped RNAs were next delivered
575 to cells by electroporation using a Gene Pulser X cell 617BR 11218 (BioRad).

576 **Co-culture of infected cells with isolated pDCs and ELISA**

577 Unless otherwise indicated, $5x10^4$ pDCs were co-cultured with $6x10^4$ PLC3 or HepG2/C3A
578 cells, electroporated or not, or as a control condition, filtered supernatants (0.4 µm). Infected
579 cells were electroporated for 48, 72 or 144 hours (as indicated) in a 200 mL final volume in
580 96-well round-bottom plates incubated at 37°C/5% CO_2. When indicated, cells were co-
581 cultured in 96-well format transwell chambers (Corning) with a 0.4 µm permeable membrane.
582 Sixteen to eighteen hours later (as specified), cell-culture supernatants were collected and the
583 levels of IFNα were measured using a commercially available specific ELISA kit (PBL
584 Interferon Source) with an assay range of 12.5-500 pg/ml.

585 **Flow cytometry-based viral spread assays.**

586 PLC3 cells were transduced with lentiviral-based vector pseudotyped with vesicular stomatitis
587 virus (VSV) glycoprotein to stably express GFP. After immuno-isolation, pDCs were stained
588 for 20 minutes at 37°C in the dark. Labeled pDCs were then spun down and re-suspended in
589 pDC culture medium. $5x10^4$ pDCs were co-cultured with $3x10^4$ HEV-infected cells
590 (electroporated 6 days prior to co-culture) and with $3x10^4$ GFP^+ uninfected cells for 48 hours
591 at 37°C/5% CO_2. The level of viral spread from HEV-infected cells ($ORF2^+$) to uninfected
592 cells (GFP^+) during co-culture was determined by flow cytometric analysis as the frequency of
593 infected cells ($ORF2^+/GFP^+$ population) among the GFP^+ cell population and similarly in GFP^-
594 populations. At the indicated times, harvested cells were resuspended using 0.48 mM EDTA-

PBS solution for the co-culture with pDCs. Cells were then incubated with 1 µL/mL viability marker diluted in PBS for 20 minutes at RT. Cytoperm/Cytofix^{TM} and permeabilization-wash solutions (BD Bioscience) were used in the subsequent stages of the ORF2 staining protocol optimized in-house for flow cytometry. Cells were fixed with Cytofix for 20 minutes at 4°C and were then washed twice and resuspended in 1x Permwash. The fixed cells were treated with cold methanol (-20°C) for 45 minutes and washed twice with 1x Permwash. The cells were then incubated with 1E6 anti-HEV antibody for a minimum of 3 hours. After another wash, cells were incubated with a secondary antibody for 2 hours. The samples were acquired after final two washes. Flow cytometer analysis was performed using a Canto II Becton Dickinson using BD FACSDIVA v8.1 software and the data were analyzed using Flow Jo 10.8.1 software (Tree Star). CellTrace Violet (CTV) Cell Proliferation kit (Life Technologies) was used to stain pDCs. LIVE/DEAD™ Fixable Near-IR - Dead Cell Stain Kit (Thermo Fisher Scientific ref #L10119) was used to check viability.

Microscopy and analysis of images.

At 4 hours post-co-culture, CTV-stained-pDCs and infected PLC3 and HepG2/C3A cells were fixed with PFA 4%, followed by immunostaining using anti-ORF2 P3H2 antibodies with a protocol optimized previously **(Bentaleb et al., 2022)**. Confocal imaging was performed using Zeiss LSM980 scanning confocal microscopy. Co-cultured cells were automatically segmented based on the CMPTx staining for cell line used and CTV labeling for pDCs. Next, the infected cells were identified by ORF2 expression, and number/frequency of infected cells were quantified using one of two similar versions of a home-made ImageJ macro (https://github.com/jbrocardplatim/PDC-contacts), adapted to HepG2/C3A or PLC3 cells. The frequency of pDCs within 3 microns of any cell was calculated, as well as the number of pDCs within 3 microns of any infected cell (from 0 to 3+). An additional macro was also used to measure the frequency of pDCs closer than 1 micron to infected cells and/or in direct contact; the individual contact areas (in µm²) were measured as well (https://github.com/jbrocardplatim/PDC-contacts). The calculation formula for contact frequencies considered variations in the number of infected cells to mitigate potential biases.

$$\frac{\text{Number of pDC-infected cell contact}}{\text{Isolated pDCs+ isolated infected cells+ pDC-infected cell contact}}$$

627 To compare the ORF2 localization in mutants and wild-type bearing cells, nuclei were stained
628 with NucSpot® Live 650 (Biotium, Catalog#40082) and HEV-ORF2 was stained with 1E6
629 antibody. For all microscopy experiments, cells were seeded in 96-Well Optical-Bottom Plate
630 (Thermo Fisher Scientific), coated with poly-L-lysine (P6282, Sigma-Aldrich).

631 **Western blotting and immunoprecipitation analyses**

632

633 Western blotting (WB) and immunoprecipitation (IP) analyses were performed as described
634 previously **(Bentaleb et al., 2022).** For WB, supernatants and lysates of WT and STOP
635 expressing PLC3 cells were heated for 20 min at 80 °C in the presence of reducing Laemmli
636 buffer. Samples were then separated by 10% SDS-PAGE and transferred onto nitrocellulose
637 membranes (Hybond-ECL, Amersham). ORF2 proteins were detected with 1E6 antibody and
638 peroxidase-conjugated anti-mouse antibodies. The detection of proteins was done by
639 chemiluminescence analysis (ECL, Amersham). For IP, P3H2 and P1H1 antibodies were
640 bound to M-280 Dynabeads (Thermofisher) overnight at 37°C following the manufacturer's
641 recommendations. Beads were washed and then incubated for 1h at room temperature with
642 supernatants (heat-inactivated) or cell lysates. Beads were washed and then heated at 80°C for
643 20 min in reducing Laemmli buffer. ORF2 proteins were detected by WB using the 1E6
644 antibody.

645
646 **Statistical analysis**
647

648 Statistical analysis was performed using R software environment for statistical computing and
649 graphics (version 3.3.2). For quantifications by ELISA, RT-qPCR, and flow cytometry,
650 analyses were performed using Wilcoxon rank-sum exact test and P value adjustment method:
651 Bonferroni or FDR was applied when mentioned. The figures were prepared using PRISM
652 software (version 10.2.1).

653
654
655
656
657
658
659
660
661
662
663

664 **Figure legends**

665

666 **Figure 1. Immuno-responsiveness of cell types selected as highly susceptible to HEV**
667 **infection. (A-C)** Quantification of transcript expression levels of representatives of IFN-I/λ-
668 related pathway, *i.e., MxA and ISG15*, NF-KB-induced signaling, *i.e., TNF* and *IL-6*, upon
669 stimulation by agonists of TLR-3 *i.e.,* addition of poly(I:C); RIG-I/MDA-5 cytosolic sensors
670 by transfection of LMW poly(I:C) and addition of recombinant IFN-β, IFN-λ3, TNF at the
671 indicated concentrations for 6 hour-incubation, determined by RT-qPCR. Analyses were
672 performed in Huh-7.5 cells (**A**), HepG2/C3A cells (**B**) and PLC3 cells (**C**) ; bars represent
673 mRNA copy number per µg total RNA; means ± standard deviation (SD); each dot represents
674 one independent experiment, $n = 4$ for treatments including polyI:C addition/transfection and
675 IFN-β treatment, n=3 for treatment with IFN-λ and TNF; statistical analysis using paired
676 pairwise wilcox test; *p* values as: * ≤0.05, ** ≤0.005 and *** ≤0.0005.(**D-E**) Quantification of
677 the replication levels at 6 d.p.e. by RT-qPCR detection of *HEV* RNA (amplicon/primers
678 designed in ORF2) in HepG2/C3A (**D**) and PLC3 cells (**E**), respectively; means ± SD; each
679 dot represents one independent experiment; n=4 for PLC3 cells and HepG2/C3A cells;
680 statistical analysis was done using Wilcoxon rank sum test with continuity correction and p
681 value adjustment with Bonferroni method; *p* values as: * ≤0.05, ** ≤0.005 and *** ≤0.0005.

682

683 **Figure 2. pDC response against HEV infected cells.** (**A-B**) Quantification of the transcript
684 expression levels of representatives of IFN-I/λ-signaling (*i.e., MxA, ISG15 and IFNλ1*) and NF-
685 KB-related pathway (*i.e., TNF and IL-6*) determined at 6 d.p.e. of HepG2/C3A (**A**) and PLC3
686 **(B)** cells, in the absence (left panels) or in co-culture with pDCs for 18 hours (right panels), as
687 indicated. Bars represent copy number per µg total RNA; means ± SD; each dot represents one
688 independent experiment (n=5 to 7). Statistical analysis was done using Wilcoxon rank sum test
689 with continuity correction; *p* values as: * ≤0.05, ** ≤0.005 and *** ≤0.0005. **(C-E)** pDCs were
690 co-cultured with HEV-electroporated PLC3 cells, their supernatants, in various settings or
691 treated by inhibitors, as indicated, for 18 hours. **(C)** Quantification of IFNα in supernatants of
692 pDCs co-cultured with HEV-infected PLC3 cells [HEV cells] or treated with supernatants from
693 HEV infected cells [HEV SN] *versus* in the absence of pDCs [no pDC]; the uninfected [cont]
694 cells were electroporated without HEV RNA and used as negative control. Bars represent
695 means ± SD and each dot represents one independent experiment (n=4). (**D**) Quantification of
696 IFNα in supernatants of pDCs in co-culture or separated from HEV-electroporated PLC3 cells
697 by a permeable membrane (0.4 µm) of transwell [transwell setting]. The TLR7 agonist,

698 imiquimod [IMQ] was used as positive control. Results presented as in **C**; (n=4). (**E**) Co-culture
699 of pDCs and HEV-electroporated PLC3 cells were treated by inhibitors of TLR7 [IRSS661],
700 blocking antibodies against $\alpha_L\beta_2$-integrin and ICAM-1, followed by the quantification of IFNα
701 in supernatants of the co-cultures. Results presented as in **C**; n>3 independent experiments.
702 Statistical analysis was done using Wilcoxon rank sum test with continuity correction; *p* values
703 as: * ≤0.05, ** ≤0.005 and *** ≤0.0005. **(F-G)** Quantification of HEV RNA replication levels
704 in HepG2/C3A (**F**) and PLC3(**G)** cells, in the absence or in co-culture with pDCs, as indicated;
705 means ± SD; each dot represents one independent experiment in terms of fold expression
706 compared to [no pDC] condition; (n=4) for HepG2/C3A cells and PLC3 cells. Statistical
707 analysis was done using Wilcoxon rank sum test with continuity correction and p value
708 adjustment with Bonferroni method; p values as: * ≤0.05, ** ≤0.005 and *** ≤0.0005. **(H)**
709 Fold-change in HEV-infected (ORF2+) PLC3 cells in the absence and presence of pDCs for
710 48 hours (n=4). **(I-J)** HEV-infected PLC3 cells (GFP^- $ORF2^+$) and uninfected cells (GFP^+
711 $ORF2^-$) were co-cultured in the presence and absence of pDCs for 48 hours. **(I)** Results are
712 presented as representative dot blots. (**J**) Fold-change in $ORF2^+$ GFP^- and $ORF2^+$ GFP^+ cells
713 was quantified by flow cytometry. Bars represent means ± SD and each dot per independent
714 experiment (n=5). Statistical analysis was done using Wilcoxon rank sum test with continuity
715 correction and p value adjustment with Bonferroni method; p values as: * ≤0.05, ** ≤0.005
716 and *** ≤0.0005.
717
718 **Figure 3. Impact of ORF2 nuclear localization on pDC activation by studying co-cultures**
719 **with specific HEV mutants.** Mutations were designed to inactivate: *i/* nuclear translocation of
720 ORF2 as [5R5A] mutant, *ii/* the ORF2 export from nucleus as [NES] mutant and iii/ ORF2g/c
721 secretion as [STOP] mutant. Cells harboring the [GAD] mutant that is deficient for viral
722 replication and/or uninfected [cont] cells were used as negative controls. Plasmids containing
723 the above-mentioned mutations in HEV genome *versus* WT, served as templates for *in vitro*
724 transcription into HEV RNA, then transfected in either HepG2/C3A or PLC3 cells, as
725 indicated. **(A-B)** Intracellular distribution of ORF2 (1E6 antibody) in HepG2/C3A (**A**) or PLC3
726 **(B)** cells electroporated with different mutants of HEV. (**C-D**) Quantification of HEV
727 replication levels of mutants *versus* WT in HepG2/C3A (n=4) (**C**) or PLC3 cells (n=3 to 6)
728 (**D**). Results represent HEV RNA copy number (primer/amplicon designed in *ORF2* RNA) per
729 µg total RNA, detected by RT-qPCR; bars represent means ± SD and dot represent independent
730 experiments. (**E-F**) Quantification of IFNα in supernatants of pDCs that were co-cultured with
731 cells harboring HEV with the indicated mutant genome *versus* WT, and GAD or uninfected,

732 as negative controls; for 18 hours; 6 d.p.e. of HepG2/C3A cells (n=5) (**E**) and PLC3 cells (n=3
733 to 8) (**F**); bars represent means ± SD and dot represent independent experiments. Statistical
734 analysis was done using Wilcoxon rank sum test; *p* values as: * ≤0.05, ** ≤0.005 and ***
735 ≤0.0005.
736
737 **Figure 4**. **Effect of ORF2 expression and localization on physical contacts between HEV**
738 **cells and pDCs, and pDC-mediated IFN response** (**A-E**) pDC co-cultured with HEV-
739 infected PLC3 cells 6 d.p.e, bearing the indicated mutations *versus* WT and GAD, as reference
740 and negative control, respectively. Confocal imaging of pDCs and HEV co-culture performed
741 after 4 hour-incubation. **(A)** Representative confocal stack-imaging of ORF2 immunostaining
742 (green) in infected PLC3 cells, which were stained with Cell-Tracker Red prior co-cultures
743 (CMTPX, red), combined with pDCs stained with Cell-Tracer Violet prior co-culture (CTV;
744 blue). (**B**) Frequency of HEV-infected (ORF2$^+$) PLC3 cells detected among the cells defined
745 as non-pDC (CTV$^-$/CMTPX$^+$); bars present means ± SD and each dot for independent image
746 (n=4). (**C**) Contact/proximity of PLC3 infected cells and pDCs with detection of CTV/pDCs
747 and CMTPX$^+$ ORF2$^+$/infected cells, as reference; bars present means ± SD and each dot for
748 independent image (n = 4). Statistical analysis was done using Wilcoxon rank sum
749 test; *p* values as: * ≤0.05, ** ≤0.005 and *** ≤0.0005.
750
751 **Acknowledgements**
752
753 We would like to thank ANRS-MIE for providing financial support (ANRS-MIE grant number:
754 AAP2020-2/ECTZ133955) and Université Claude Bernard Lyon 1 (UCBL1) for GJ's PhD
755 fellowship. We acknowledge Dr. Julie Lucifora, Dr. David Durantel, Dr. Elena Tomasello, Dr.
756 Alexandre Belot, Dr. Søren Riis Paludan, Dr. Marco Binder and Dr. Antoine Marçais for
757 scientific discussions. We thank SFR Biosciences (UMS3444/CNRS, US8/Inserm, ENS de
758 Lyon, UCBL) including the PLATIM and AniRA-cytometry facilities, for technical assistance
759 in imaging and FACS analyses, respectively. Special thanks to Dr. Marion Delphin and
760 Roxanne Fouille for their contribution in supporting experiments. The contribution of the EFS
761 Confluence/Decine-Lyon is also noteworthy. Finally, we thank current and former members of
762 the VIV team for helpful discussions and support: Dr. Margarida Sa Ribeiro, Célia Nuovo,
763 Matteo Agostini, and Manon Venet.
764
765

References

1. Andonov, A., Robbins, M., Borlang, J., Cao, J., Hatchette, T., Stueck, A., Deschambault, Y., Murnaghan, K., Varga, J., & Johnston, L. (2019). Rat Hepatitis E Virus Linked to Severe Acute Hepatitis in an Immunocompetent Patient. *The Journal of Infectious Diseases*, *220*(6), 951–955. https://doi.org/10.1093/infdis/jiz025
2. Ankavay, M., Montpellier, C., Sayed, I. M., Saliou, J. M., Wychowski, C., Saas, L., Duvet, S., Aliouat-Denis, C. M., Farhat, R., de Masson d'Autume, V., Meuleman, P., Dubuisson, J., & Cocquerel, L. (2019). New insights into the ORF2 capsid protein, a key player of the hepatitis E virus lifecycle. *Scientific Reports*. https://doi.org/10.1038/s41598-019-42737-2
3. Assil, S., Coléon, S., Dong, C., Décembre, E., Sherry, L., Allatif, O., Webster, B., & Dreux, M. (2019). Plasmacytoid Dendritic Cells and Infected Cells Form an Interferogenic Synapse Required for Antiviral Responses. *Cell Host and Microbe*. https://doi.org/10.1016/j.chom.2019.03.005
4. Assil, S., Futsch, N., Décembre, E., Alais, S., Gessain, A., Cosset, F.-L., Mahieux, R., Dreux, M., & Dutartre, H. (2019). Sensing of cell-associated HTLV by plasmacytoid dendritic cells is regulated by dense β-galactoside glycosylation. *PLOS Pathogens*, *15*(2), e1007589. https://doi.org/10.1371/journal.ppat.1007589
5. Bagdassarian, E., Doceul, V., Pellerin, M., Demange, A., Meyer, L., Jouvenet, N., & Pavio, N. (2018). The Amino-Terminal Region of Hepatitis E Virus ORF1 Containing a Methyltransferase (Met) and a Papain-Like Cysteine Protease (PCP) Domain Counteracts Type I Interferon Response. *Viruses*, *10*(12), 726. https://doi.org/10.3390/v10120726
6. Behrendt, P., Lüth, S., Dammermann, W., Drave, S., Brown, R. J. P., Todt, D., Schnoor, U., Steinmann, E., Wedemeyer, H., Pischke, S., & Iking-Konert, C. (2017). Exacerbation of hepatitis E virus infection during anti-TNFα treatment. *Joint Bone Spine*, *84*(2), 217–219. https://doi.org/10.1016/j.jbspin.2016.09.017
7. Bentaleb, C., Hervouet, K., Montpellier, C., Camuzet, C., Ferrié, M., Burlaud-Gaillard, J., Bressanelli, S., Metzger, K., Werkmeister, E., Ankavay, M., Janampa, N. L., Marlet, J., Roux, J., Deffaud, C., Goffard, A., Rouillé, Y., Dubuisson, J., Roingeard, P., Aliouat-Denis, C.-M., & Cocquerel, L. (2022). The endocytic recycling compartment serves as a viral factory for hepatitis E virus. *Cellular and Molecular Life Sciences*, *79*(12), 615. https://doi.org/10.1007/s00018-022-04646-y
8. Bermejo-Jambrina, M., Eder, J., Helgers, L. C., Hertoghs, N., Nijmeijer, B. M., Stunnenberg, M., & Geijtenbeek, T. B. H. (2018). C-Type Lectin Receptors in Antiviral Immunity and Viral Escape. *Frontiers in Immunology*, *9*, 590. https://doi.org/10.3389/fimmu.2018.00590
9. Blight, K. J., McKeating, J. A., & Rice, C. M. (2002). Highly Permissive Cell Lines for Subgenomic and Genomic Hepatitis C Virus RNA Replication. *Journal of Virology*, *76*(24), 13001–13014. https://doi.org/10.1128/JVI.76.24.13001-13014.2002
10. Bourdon, M., Manet, C., & Montagutelli, X. (2020). Host genetic susceptibility to viral infections: The role of type I interferon induction. *Genes & Immunity*, *21*(6–8), 365–379. https://doi.org/10.1038/s41435-020-00116-2
11. Broggi, A., Granucci, F., & Zanoni, I. (2020). Type III interferons: Balancing tissue tolerance and resistance to pathogen invasion. *Journal of Experimental Medicine*, *217*(1), e20190295. https://doi.org/10.1084/jem.20190295
12. Cambi, A., Koopman, M., & Figdor, C. G. (2005). How C-type lectins detect pathogens: C-type lectins and pathogens. *Cellular Microbiology*, *7*(4), 481–488. https://doi.org/10.1111/j.1462-5822.2005.00506.x
13. Cervantes-Barragan, L., Lewis, K. L., Firner, S., Thiel, V., Hugues, S., Reith, W., Ludewig, B., & Reizis, B. (2012). Plasmacytoid dendritic cells control T-cell response to chronic viral infection. *Proceedings of the National Academy of Sciences of the United States of America*. https://doi.org/10.1073/pnas.1117359109
14. Crouse, J., Kalinke, U., & Oxenius, A. (2015). Regulation of antiviral T cell responses by type I interferons. *Nature Reviews Immunology*, *15*(4), 231–242. https://doi.org/10.1038/nri3806
15. Devhare, P., Madiyal, M., Mukhopadhyay, C., Shetty, S., & Shastry, S. (2021). Interplay between Hepatitis E Virus and Host Cell Pattern Recognition Receptors. *International Journal of Molecular Sciences*, *22*(17), 9259. https://doi.org/10.3390/ijms22179259
16. Doceul, V., Bagdassarian, E., Demange, A., & Pavio, N. (2016). Zoonotic Hepatitis E Virus: Classification, Animal Reservoirs and Transmission Routes. *Viruses*, *8*(10), 270. https://doi.org/10.3390/v8100270
17. Dong, C., Zafrullah, M., Mixson-Hayden, T., Dai, X., Liang, J., Meng, J., & Kamili, S. (2012). Suppression of interferon-α signaling by hepatitis E virus. *Hepatology*, *55*(5), 1324–1332. https://doi.org/10.1002/hep.25530
18. Doyle, E. H., Rahman, A., Aloman, C., Klepper, A. L., El-Shamy, A., Eng, F., Rocha, C., Kim, S., Haydel, B., Florman, S. S., Fiel, M. I., Schiano, T., & Branch, A. D. (2019). Individual liver plasmacytoid dendritic cells are capable of producing IFNα and multiple additional cytokines during chronic HCV infection. *PLOS Pathogens*, *15*(7), e1007935. https://doi.org/10.1371/journal.ppat.1007935
19. Dreux, M., Garaigorta, U., Boyd, B., Décembre, E., Chung, J., Whitten-Bauer, C., Wieland, S., & Chisari, F. V. (2012). Short-Range Exosomal Transfer of Viral RNA from Infected Cells to Plasmacytoid Dendritic Cells Triggers Innate Immunity. *Cell Host & Microbe*, *12*(4), 558–570. https://doi.org/10.1016/j.chom.2012.08.010
20. Emerson, S. U., Nguyen, H. T., Torian, U., Mather, K., & Firth, A. E. (2013). An essential RNA element resides in a central region of hepatitis E virus ORF2. *Journal of General Virology*, *94*(7), 1468–1476. https://doi.org/10.1099/vir.0.051870-0
21. Florentin, J., Aouar, B., Dental, C., Thumann, C., Firaguay, G., Gondois-Rey, F., Soumelis, V., Baumert, T. F., Nunès, J. A., Olive, D., Hirsch, I., & Stranska, R. (2012). HCV glycoprotein E2 is a novel BDCA-2 ligand and acts as an inhibitor of IFN production by plasmacytoid dendritic cells. *Blood*, *120*(23), 4544–4551. https://doi.org/10.1182/blood-2012-02-413286
22. Gibson, S. J., Lindh, J. M., Riter, T. R., Gleason, R. M., Rogers, L. M., Fuller, A. E., Oesterich, J. L., Gorden, K. B., Qiu, X., McKane, S. W., Noelle, R. J., Miller, R. L., Kedl, R. M., Fitzgerald-Bocarsly, P., Tomai, M. A., & Vasilakos, J. P. (2002). Plasmacytoid dendritic cells produce cytokines and mature in response to the TLR7 agonists, imiquimod and resiquimod. *Cellular Immunology*, *218*(1–2), 74–86. https://doi.org/10.1016/S0008-8749(02)00517-8

23. Gilliet, M., Cao, W., & Liu, Y.-J. (2008). Plasmacytoid dendritic cells: Sensing nucleic acids in viral infection and autoimmune diseases. *Nature Reviews Immunology*, *8*(8), 594–606. https://doi.org/10.1038/nri2358

24. Graff, J., Torian, U., Nguyen, H., & Emerson, S. U. (2006). A Bicistronic Subgenomic mRNA Encodes both the ORF2 and ORF3 Proteins of Hepatitis E Virus. *Journal of Virology*, *80*(12), 5919–5926. https://doi.org/10.1128/JVI.00046-06

25. Grange, Z. L., Goldstein, T., Johnson, C. K., Anthony, S., Gilardi, K., Daszak, P., Olival, K. J., O'Rourke, T., Murray, S., Olson, S. H., Togami, E., Vidal, G., Expert Panel, PREDICT Consortium, Mazet, J. A. K., Anderson, K., Auewarakul, P., Coffey, L., Corley, R., … Fine, A. (2021). Ranking the risk of animal-to-human spillover for newly discovered viruses. *Proceedings of the National Academy of Sciences*, *118*(15), e2002324118. https://doi.org/10.1073/pnas.2002324118

26. Gu, J., Isaji, T., Xu, Q., Kariya, Y., Gu, W., Fukuda, T., & Du, Y. (2012). Potential roles of N-glycosylation in cell adhesion. *Glycoconjugate Journal*, *29*(8–9), 599–607. https://doi.org/10.1007/s10719-012-9386-1

27. Hervouet, K., Ferrié, M., Ankavay, M., Montpellier, C., Camuzet, C., Alexandre, V., Dembélé, A., Lecoeur, C., Foe, A. T., Bouquet, P., Hot, D., Vausselin, T., Saliou, J.-M., Salomé-Desnoulez, S., Vandeputte, A., Marsollier, L., Brodin, P., Dreux, M., Rouillé, Y., … Cocquerel, L. (2022). An Arginine-Rich Motif in the ORF2 capsid protein regulates the hepatitis E virus lifecycle and interactions with the host cell. *PLOS Pathogens*, *18*(8), e1010798. https://doi.org/10.1371/journal.ppat.1010798

28. Knowles, B. B., Howe, C. C., & Aden, D. P. (1980). Human Hepatocellular Carcinoma Cell Lines Secrete the Major Plasma Proteins and Hepatitis B Surface Antigen. *Science*, *209*(4455), 497–499. https://doi.org/10.1126/science.6248960

29. Koonin, E. V., Gorbalenya, A. E., Purdy, M. A., Rozanov, M. N., Reyes, G. R., & Bradley, D. W. (1992). Computer-assisted assignment of functional domains in the nonstructural polyprotein of hepatitis E virus: Delineation of an additional group of positive-strand RNA plant and animal viruses. *Proceedings of the National Academy of Sciences*, *89*(17), 8259–8263. https://doi.org/10.1073/pnas.89.17.8259

30. Lazear, H. M., Schoggins, J. W., & Diamond, M. S. (2019). Shared and Distinct Functions of Type I and Type III Interferons. *Immunity*, *50*(4), 907–923. https://doi.org/10.1016/j.immuni.2019.03.025

31. Lee, G.-H., Tan, B.-H., Chi-Yuan Teo, E., Lim, S.-G., Dan, Y.-Y., Wee, A., Kim Aw, P. P., Zhu, Y., Hibberd, M. L., Tan, C.-K., Purdy, M. A., & Teo, C.-G. (2016). Chronic Infection With Camelid Hepatitis E Virus in a Liver Transplant Recipient Who Regularly Consumes Camel Meat and Milk. *Gastroenterology*, *150*(2), 355-357.e3. https://doi.org/10.1053/j.gastro.2015.10.048

32. Lei, Q., Li, L., Zhang, S., Li, T., Zhang, X., Ding, X., & Qin, B. (2018). HEV ORF3 downregulates TLR7 to inhibit the generation of type I interferon via impairment of multiple signaling pathways. *Scientific Reports*, *8*(1), 8585. https://doi.org/10.1038/s41598-018-26975-4

33. Lenggenhager, D., Gouttenoire, J., Malehmir, M., Bawohl, M., Honcharova-Biletska, H., Kreutzer, S., Semela, D., Neuweiler, J., Hürlimann, S., Aepli, P., Fraga, M., Sahli, R., Terracciano, L., Rubbia-Brandt, L., Müllhaupt, B., Sempoux, C., Moradpour, D., & Weber, A. (2017). Visualization of hepatitis E virus RNA and proteins in the human liver. *Journal of Hepatology*, *67*(3), 471–479. https://doi.org/10.1016/j.jhep.2017.04.002

34. Lhomme, S., Marion, O., Abravanel, F., Izopet, J., & Kamar, N. (2020). Clinical Manifestations, Pathogenesis and Treatment of Hepatitis E Virus Infections. *Journal of Clinical Medicine*, *9*(2), 331. https://doi.org/10.3390/jcm9020331

35. Li, P., Liu, J., Li, Y., Su, J., Ma, Z., Bramer, W. M., Cao, W., De Man, R. A., Peppelenbosch, M. P., & Pan, Q. (2020). The global epidemiology of hepatitis E virus infection: A systematic review and meta-analysis. *Liver International*, *40*(7), 1516–1528. https://doi.org/10.1111/liv.14468

36. Lin, S., Yang, Y., Nan, Y., Ma, Z., Yang, L., & Zhang, Y.-J. (2019). The Capsid Protein of Hepatitis E Virus Inhibits Interferon Induction via Its N-Terminal Arginine-Rich Motif. *Viruses*, *11*(11), 1050. https://doi.org/10.3390/v11111050

37. Ma, N., Lu, J., Pei, Y., & Robertson, E. S. (2022). Transcriptome reprogramming of Epstein-Barr virus infected epithelial and B cells reveals distinct host-virus interaction profiles. *Cell Death & Disease*, *13*(10), 894. https://doi.org/10.1038/s41419-022-05327-1

38. Ma, Z., De Man, R. A., Kamar, N., & Pan, Q. (2022). Chronic hepatitis E: Advancing research and patient care. *Journal of Hepatology*, *77*(4), 1109–1123. https://doi.org/10.1016/j.jhep.2022.05.006

39. MacNab, G. M., Alexander, J. J., Lecatsas, G., Bey, E. M., & Urbanowicz, J. M. (1976). Hepatitis B surface antigen produced by a human hepatoma cell line. *British Journal of Cancer*, *34*(5), 509–515. https://doi.org/10.1038/bjc.1976.205

40. Marlin, S. D., & Springer, T. A. (1987). Purified intercellular adhesion molecule-1 (ICAM-1) is a ligand for lymphocyte function-associated antigen 1 (LFA-1). *Cell*, *51*(5), 813–819. https://doi.org/10.1016/0092-8674(87)90104-8

41. Meyer-Wentrup, F., Benitez-Ribas, D., Tacken, P. J., Punt, C. J. A., Figdor, C. G., De Vries, I. J. M., & Adema, G. J. (2008). Targeting DCIR on human plasmacytoid dendritic cells results in antigen presentation and inhibits IFN-α production. *Blood*, *111*(8), 4245–4253. https://doi.org/10.1182/blood-2007-03-081398

42. Moal, V., Textoris, J., Ben Amara, A., Mehraj, V., Berland, Y., Colson, P., & Mege, J.-L. (2013). Chronic Hepatitis E Virus Infection Is Specifically Associated With an Interferon-Related Transcriptional Program. *The Journal of Infectious Diseases*, *207*(1), 125–132. https://doi.org/10.1093/infdis/jis632

43. Montpellier, C., Wychowski, C., Sayed, I. M., Meunier, J.-C., Saliou, J.-M., Ankavay, M., Bull, A., Pillez, A., Abravanel, F., Helle, F., Brochot, E., Drobecq, H., Farhat, R., Aliouat-Denis, C.-M., Haddad, J. G., Izopet, J., Meuleman, P., Goffard, A., Dubuisson, J., & Cocquerel, L. (2018). Hepatitis E Virus Lifecycle and Identification of 3 Forms of the ORF2 Capsid Protein. *Gastroenterology*, *154*(1), 211-223.e8. https://doi.org/10.1053/j.gastro.2017.09.020

44. Murata, K., Kang, J.-H., Nagashima, S., Matsui, T., Karino, Y., Yamamoto, Y., Atarashi, T., Oohara, M., Uebayashi, M., Sakata, H., Matsubayashi, K., Takahashi, K., Arai, M., Mishiro, S., Sugiyama, M., Mizokami, M., & Okamoto, H. (2020). IFN-λ3 as a host immune response in acute hepatitis E virus infection. *Cytokine*, *125*, 154816. https://doi.org/10.1016/j.cyto.2019.154816

45. Nagashima, S., Primadharsini, P. P., Nishiyama, T., Takahashi, M., Murata, K., & Okamoto, H. (2023). Development of a HiBiT-tagged reporter hepatitis E virus and its utility as an antiviral drug screening platform. *Journal of Virology*, *97*(9), e00508-23. https://doi.org/10.1128/jvi.00508-23

46. Nan, Y., Yu, Y., Ma, Z., Khattar, S. K., Fredericksen, B., & Zhang, Y.-J. (2014). Hepatitis E Virus Inhibits Type I Interferon Induction by ORF1 Products. *Journal of Virology*. https://doi.org/10.1128/jvi.01935-14

47. Nimgaonkar, I., Ding, Q., Schwartz, R. E., & Ploss, A. (2018). Hepatitis E virus: Advances and challenges. *Nature Reviews Gastroenterology & Hepatology*, *15*(2), 96–110. https://doi.org/10.1038/nrgastro.2017.150

48. Ohtsubo, K., & Marth, J. D. (2006). Glycosylation in Cellular Mechanisms of Health and Disease. *Cell*, *126*(5), 855–867. https://doi.org/10.1016/j.cell.2006.08.019

49. Parr, M. B., & Parr, E. L. (2000). Interferon-γ up-regulates intercellular adhesion molecule-1 and vascular cell adhesion molecule-1 and recruits lymphocytes into the vagina of immune mice challenged with herpes simplex virus-2. *Immunology*, *99*(4), 540–545. https://doi.org/10.1046/j.1365-2567.2000.00980.x

50. Ralfs, P., Holland, B., Salinas, E., Bremer, B., Wang, M., Zhu, J., Ambardekar, C., Blasczyk, H., Walker, C. M., Feng, Z., & Grakoui, A. (2023). Soluble ORF2 protein enhances HEV replication and induces long-lasting antibody response and protective immunity in vivo. *Hepatology*, *78*(6), 1867–1881. https://doi.org/10.1097/HEP.0000000000000421

51. Reglero-Real, N., Álvarez-Varela, A., Cernuda-Morollón, E., Feito, J., Marcos-Ramiro, B., Fernández-Martín, L., Gómez-Lechón, M. J., Muntané, J., Sandoval, P., Majano, P. L., Correas, I., Alonso, M. A., & Millán, J. (2014). Apicobasal Polarity Controls Lymphocyte Adhesion to Hepatic Epithelial Cells. *Cell Reports*, *8*(6), 1879–1893. https://doi.org/10.1016/j.celrep.2014.08.007

52. Rehwinkel, J., & Gack, M. U. (2020). RIG-I-like receptors: Their regulation and roles in RNA sensing. *Nature Reviews Immunology*, *20*(9), 537–551. https://doi.org/10.1038/s41577-020-0288-3

53. Reizis, B. (2019). Plasmacytoid Dendritic Cells: Development, Regulation, and Function. *Immunity*, *50*(1), 37–50. https://doi.org/10.1016/j.immuni.2018.12.027

54. Sari, G., Mulders, C. E., Zhu, J., Van Oord, G. W., Feng, Z., Kreeft-Voermans, J. J. C., Boonstra, A., & Vanwolleghem, T. (2021). Treatment induced clearance of hepatitis E viruses by interferon-lambda in liver-humanized mice. *Liver International*, *41*(12), 2866–2873. https://doi.org/10.1111/liv.15033

55. Sayed, I. M., Verhoye, L., Cocquerel, L., Abravanel, F., Foquet, L., Montpellier, C., Debing, Y., Farhoudi, A., Wychowski, C., Dubuisson, J., Leroux-Roels, G., Neyts, J., Izopet, J., Michiels, T., & Meuleman, P. (2017). Study of hepatitis E virus infection of genotype 1 and 3 in mice with humanised liver. *Gut*, *66*(5), 920–929. https://doi.org/10.1136/gutjnl-2015-311109

56. Schemmerer, M., Apelt, S., Trojnar, E., Ulrich, R. G., Wenzel, J. J., & Johne, R. (2016). Enhanced replication of hepatitis E virus strain 47832C in an A549-derived subclonal cell line. *Viruses*. https://doi.org/10.3390/v8100267

57. Schneider, W. M., Chevillotte, M. D., & Rice, C. M. (2014). Interferon-Stimulated Genes: A Complex Web of Host Defenses. *Annual Review of Immunology*, *32*(1), 513–545. https://doi.org/10.1146/annurev-immunol-032713-120231

58. Shukla, P., Nguyen, H. T., Faulk, K., Mather, K., Torian, U., Engle, R. E., & Emerson, S. U. (2012). Adaptation of a Genotype 3 Hepatitis E Virus to Efficient Growth in Cell Culture Depends on an Inserted Human Gene Segment Acquired by Recombination. *Journal of Virology*, *86*(10), 5697–5707. https://doi.org/10.1128/JVI.00146-12

59. Shukla, P., Nguyen, H. T., Torian, U., Engle, R. E., Faulk, K., Dalton, H. R., Bendall, R. P., Keane, F. E., Purcell, R. H., & Emerson, S. U. (2011). Cross-species infections of cultured cells by hepatitis E virus and discovery of an infectious virus-host recombinant. *Proceedings of the National Academy of Sciences of the United States of America*. https://doi.org/10.1073/pnas.1018878108

60. Silvin, A., Yu, C. I., Lahaye, X., Imperatore, F., Brault, J.-B., Cardinaud, S., Becker, C., Kwan, W.-H., Conrad, C., Maurin, M., Goudot, C., Marques-Ladeira, S., Wang, Y., Pascual, V., Anguiano, E., Albrecht, R. A., Iannacone, M., García-Sastre, A., Goud, B., … Manel, N. (2017). Constitutive resistance to viral infection in human CD141 $^{+}$ dendritic cells. *Science Immunology*, *2*(13), eaai8071. https://doi.org/10.1126/sciimmunol.aai8071

61. Songtanin, B., Molehin, A. J., Brittan, K., Manatsathit, W., & Nugent, K. (2023). Hepatitis E Virus Infections: Epidemiology, Genetic Diversity, and Clinical Considerations. *Viruses*, *15*(6), 1389. https://doi.org/10.3390/v15061389

62. Sridhar, S., Yip, C. C. Y., Wu, S., Cai, J., Zhang, A. J.-X., Leung, K.-H., Chung, T. W. H., Chan, J. F. W., Chan, W.-M., Teng, J. L. L., Au-Yeung, R. K. H., Cheng, V. C. C., Chen, H., Lau, S. K. P., Woo, P. C. Y., Xia, N.-S., Lo, C.-M., & Yuen, K.-Y. (2018). Rat Hepatitis E Virus as Cause of Persistent Hepatitis after Liver Transplant. *Emerging Infectious Diseases*, *24*(12), 2241–2250. https://doi.org/10.3201/eid2412.180937

63. Sumpter, R., Loo, Y.-M., Foy, E., Li, K., Yoneyama, M., Fujita, T., Lemon, S. M., & Gale, M. (2005). Regulating Intracellular Antiviral Defense and Permissiveness to Hepatitis C Virus RNA Replication through a Cellular RNA Helicase, RIG-I. *Journal of Virology*, *79*(5), 2689–2699. https://doi.org/10.1128/JVI.79.5.2689-2699.2005

64. Swiecki, M., Gilfillan, S., Vermi, W., Wang, Y., & Colonna, M. (2010). Plasmacytoid Dendritic Cell Ablation Impacts Early Interferon Responses and Antiviral NK and CD8+ T Cell Accrual. *Immunity*. https://doi.org/10.1016/j.immuni.2010.11.020

65. Tam, A. W., Smith, M. M., Guerra, M. E., Huang, C.-C., Bradley, D. W., Fry, K. E., & Reyes, G. R. (1991). Hepatitis E virus (HEV): Molecular cloning and sequencing of the full-length viral genome. *Virology*, *185*(1), 120–131. https://doi.org/10.1016/0042-6822(91)90760-9

66. Todt, D., François, C., Anggakusuma, Behrendt, P., Engelmann, M., Knegendorf, L., Vieyres, G., Wedemeyer, H., Hartmann, R., Pietschmann, T., Duverlie, G., & Steinmann, E. (2016). Antiviral Activities of Different Interferon Types and Subtypes against Hepatitis E Virus Replication. *Antimicrobial Agents and Chemotherapy*, *60*(4), 2132–2139. https://doi.org/10.1128/AAC.02427-15

67. Venet, M., Ribeiro, M. S., Décembre, E., Bellomo, A., Joshi, G., Nuovo, C., Villard, M., Cluet, D., Perret, M., Pescamona, R., Paidassi, H., Walzer, T., Allatif, O., Belot, A., Trouillet-Assant, S., Ricci, E. P., & Dreux, M. (2023). Severe COVID-19 patients have impaired plasmacytoid dendritic cell-mediated control of SARS-CoV-2. *Nature Communications*, *14*(1), 694. https://doi.org/10.1038/s41467-023-36140-9

68. Wang, W., Xu, L., Brandsma, J. H., Wang, Y., Hakim, M. S., Zhou, X., Yin, Y., Fuhler, G. M., Van Der Laan, L. J. W., Van Der Woude, C. J., Sprengers, D., Metselaar, H. J., Smits, R., Poot, R. A., Peppelenbosch, M. P., & Pan, Q. (2016). Convergent Transcription of Interferon-stimulated Genes by TNF-α and IFN-α Augments Antiviral Activity against HCV and HEV. *Scientific Reports*, *6*(1), 25482. https://doi.org/10.1038/srep25482

69. Webster, B., Assil, S., & Dreux, M. (2016). Cell-Cell Sensing of Viral Infection by Plasmacytoid Dendritic Cells. *Journal of Virology*. https://doi.org/10.1128/jvi.01692-16

70. Webster, B., Werneke, S. W., Zafirova, B., This, S., Coléon, S., Décembre, E., Paidassi, H., Bouvier, I., Joubert, P.-E., Duffy, D., Walzer, T., Albert, M. L., & Dreux, M. (2018). Plasmacytoid dendritic cells control dengue and Chikungunya virus infections via IRF7-regulated interferon responses. *eLife*, *7*, e34273. https://doi.org/10.7554/eLife.34273

71. Wu, X., Dao Thi, V. L., Liu, P., Takacs, C. N., Xiang, K., Andrus, L., Gouttenoire, J., Moradpour, D., & Rice, C. M. (2018). Pan-Genotype Hepatitis E Virus Replication in Stem Cell–Derived Hepatocellular Systems. *Gastroenterology*, *154*(3), 663-674.e7. https://doi.org/10.1053/j.gastro.2017.10.041

72. Yarilina, A., Park-Min, K.-H., Antoniv, T., Hu, X., & Ivashkiv, L. B. (2008). TNF activates an IRF1-dependent autocrine loop leading to sustained expression of chemokines and STAT1-dependent type I interferon–response genes. *Nature Immunology*, *9*(4), 378–387. https://doi.org/10.1038/ni1576

73. Yin, X., Li, X., Ambardekar, C., Hu, Z., Lhomme, S., & Feng, Z. (2017). Hepatitis E virus persists in the presence of a type III interferon response. *PLOS Pathogens*, *13*(5), e1006417. https://doi.org/10.1371/journal.ppat.1006417

74. Yin, X., Ying, D., Lhomme, S., Tang, Z., Walker, C. M., Xia, N., Zheng, Z., & Feng, Z. (2018). Origin, antigenicity, and function of a secreted form of ORF2 in hepatitis E virus infection. *Proceedings of the National Academy of Sciences of the United States of America*. https://doi.org/10.1073/pnas.1721345115

75. Yu, C., Boon, D., McDonald, S. L., Myers, T. G., Tomioka, K., Nguyen, H., Engle, R. E., Govindarajan, S., Emerson, S. U., & Purcell, R. H. (2010). Pathogenesis of Hepatitis E Virus and Hepatitis C Virus in Chimpanzees: Similarities and Differences. *Journal of Virology*, *84*(21), 11264–11278. https://doi.org/10.1128/JVI.01205-10

76. Yun, T. J., Igarashi, S., Zhao, H., Perez, O. A., Pereira, M. R., Zorn, E., Shen, Y., Goodrum, F., Rahman, A., Sims, P. A., Farber, D. L., & Reizis, B. (2021). Human plasmacytoid dendritic cells mount a distinct antiviral response to virus-infected cells. *Science Immunology*, *6*(58), eabc7302. https://doi.org/10.1126/sciimmunol.abc7302

77. Zhong, P., Agosto, L. M., Ilinskaya, A., Dorjbal, B., Truong, R., Derse, D., Uchil, P. D., Heidecker, G., & Mothes, W. (2013). Cell-to-Cell Transmission Can Overcome Multiple Donor and Target Cell Barriers Imposed on Cell-Free HIV. *PLoS ONE*, *8*(1), e53138. https://doi.org/10.1371/journal.pone.0053138

78. Zhou, X., Xu, L., Wang, W., Watashi, K., Wang, Y., Sprengers, D., De Ruiter, P. E., Van Der Laan, L. J. W., Metselaar, H. J., Kamar, N., Peppelenbosch, M. P., & Pan, Q. (2016). Disparity of basal and therapeutically activated interferon signalling in constraining hepatitis E virus infection. *Journal of Viral Hepatitis*, *23*(4), 294–304. https://doi.org/10.1111/jvh.12491

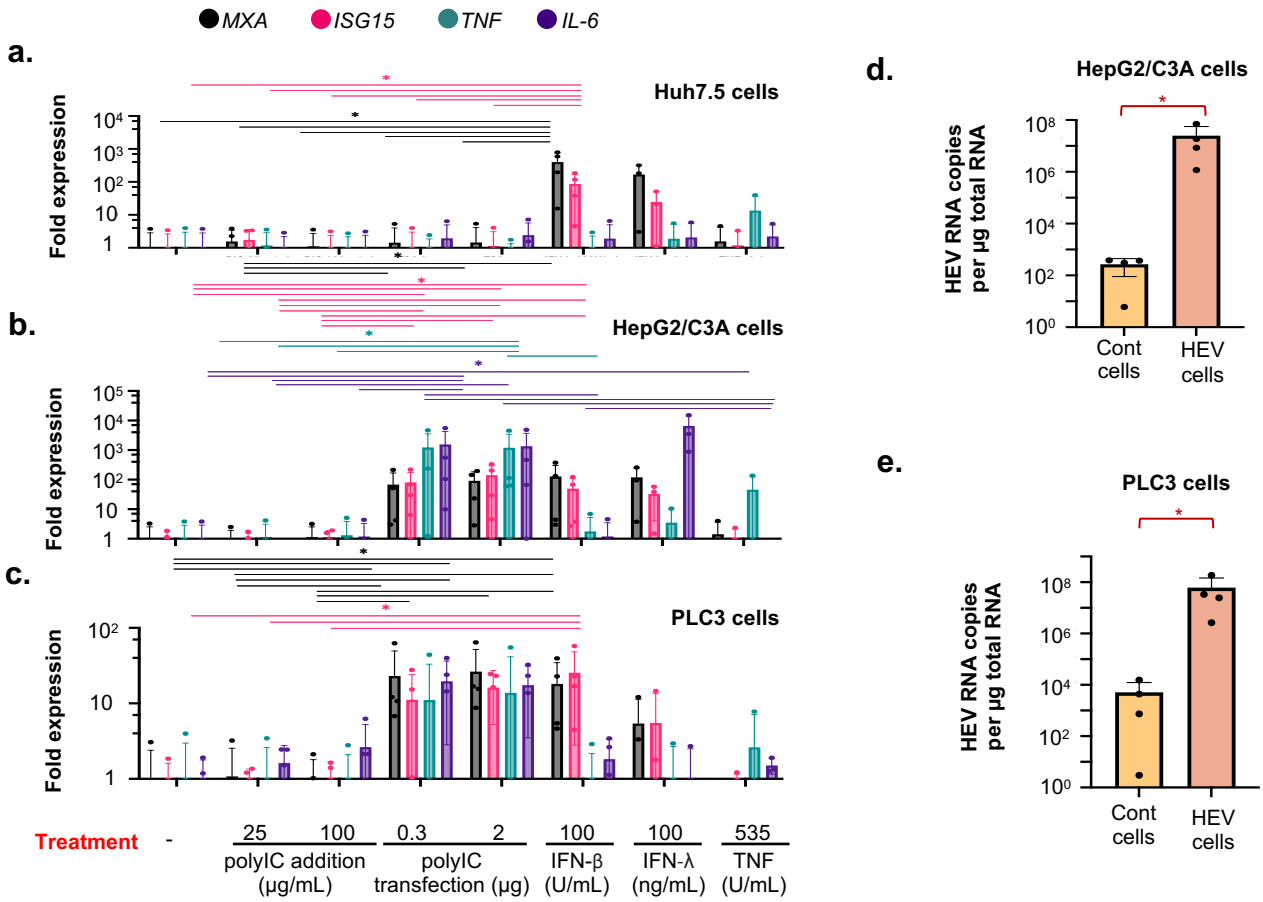
MXA
ISG15
TNF
IL-6
a.
Huh7.5 cells
Fold expression
b.
HepG2/C3A cells
Fold expression
c.
PLC3 cells
Fold expression
Treatment
-
25
100
polyIC addition (µg/mL)
0.3
2
polyIC transfection (µg)
100
IFN-β (U/mL)
100
IFN-λ (ng/mL)
535
TNF (U/mL)
d.
HepG2/C3A cells
HEV RNA copies per µg total RNA
Cont cells
HEV cells
e.
PLC3 cells
HEV RNA copies per µg total RNA
Cont cells
HEV cells

Figure 1

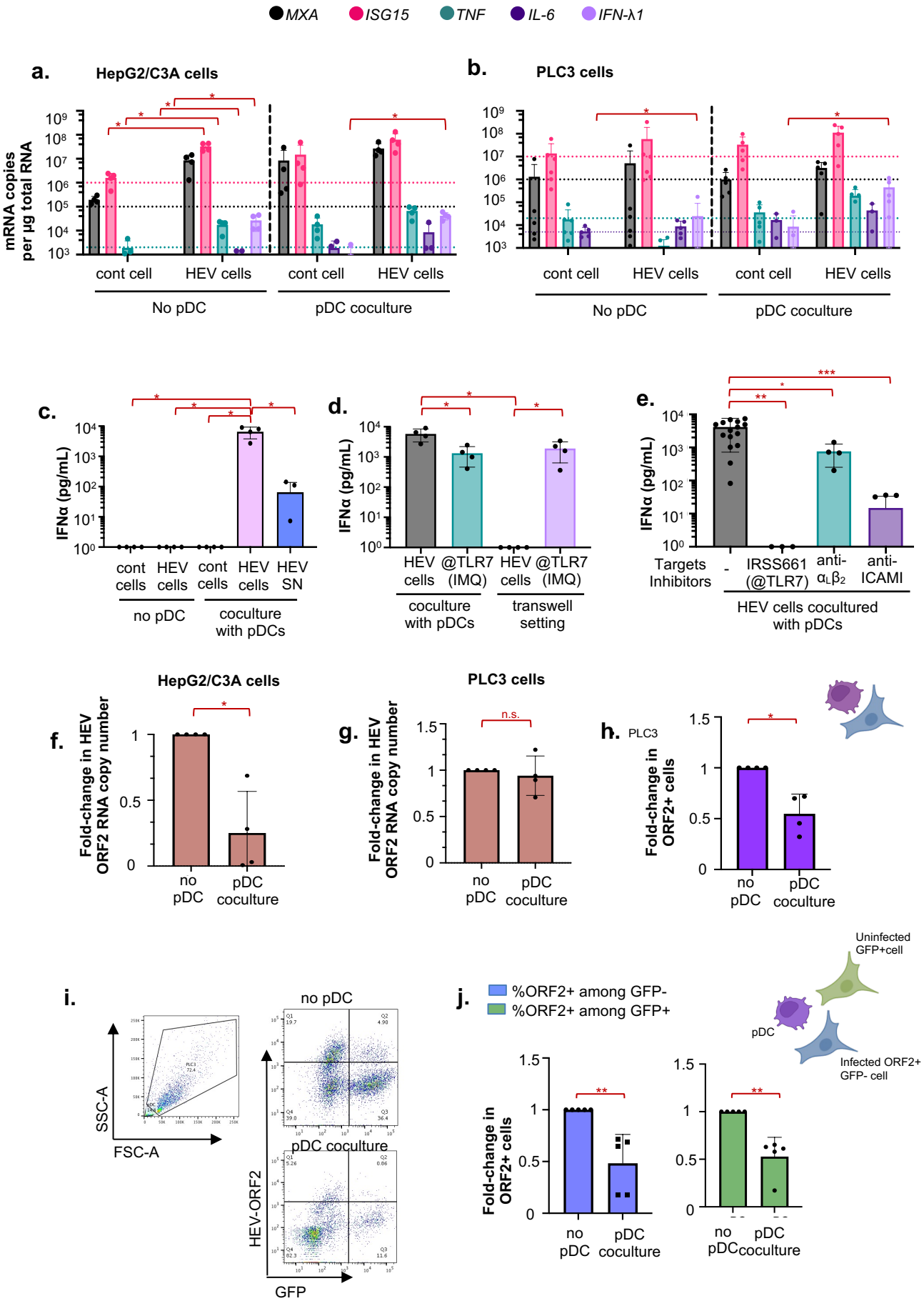
MXA
ISG15
TNF
IL-6
IFN-λ1
a.
HepG2/C3A cells
mRNA copies per µg total RNA
cont cell
HEV cells
No pDC
pDC coculture
b.
PLC3 cells
c.
IFNα (pg/mL)
cont cells
HEV cells
HEV SN
no pDC
coculture with pDCs
d.
HEV cells
@TLR7 (IMQ)
coculture with pDCs
transwell setting
e.
Targets
Inhibitors
IRSS661 (@TLR7)
anti-αLβ2
anti-ICAMI
HEV cells cocultured with pDCs
f.
Fold-change in HEV ORF2 RNA copy number
no pDC
pDC coculture
g.
n.s.
h.
PLC3
Fold-change in ORF2+ cells
i.
SSC-A
FSC-A
no pDC
pDC coculture
HEV-ORF2
GFP
j.
%ORF2+ among GFP-
%ORF2+ among GFP+
Uninfected GFP+cell
pDC
Infected ORF2+ GFP- cell

Figure 2

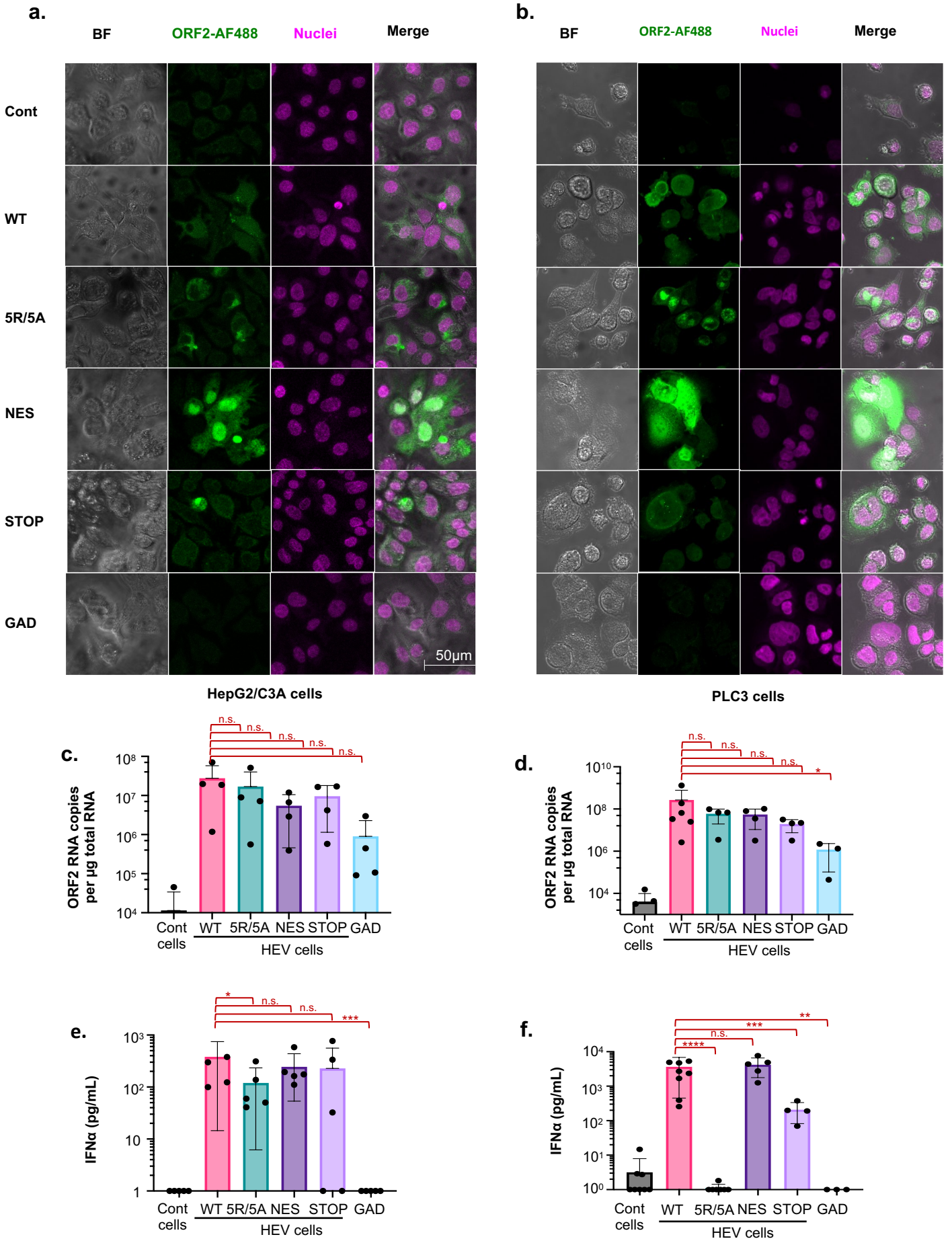
a.
BF
ORF2-AF488
Nuclei
Merge
Cont
WT
5R/5A
NES
STOP
GAD
50µm
HepG2/C3A cells
b.
BF
ORF2-AF488
Nuclei
Merge
PLC3 cells
c.
ORF2 RNA copies per µg total RNA
n.s.
Cont cells
WT 5R/5A NES STOP GAD
HEV cells
d.
ORF2 RNA copies per µg total RNA
n.s.
*
Cont cells
WT 5R/5A NES STOP GAD
HEV cells
e.
IFNα (pg/mL)
*
n.s.
***
Cont cells
WT 5R/5A NES STOP GAD
HEV cells
f.
IFNα (pg/mL)
****
n.s.
***
**
Cont cells
WT 5R/5A NES STOP GAD
HEV cells

Figure 3

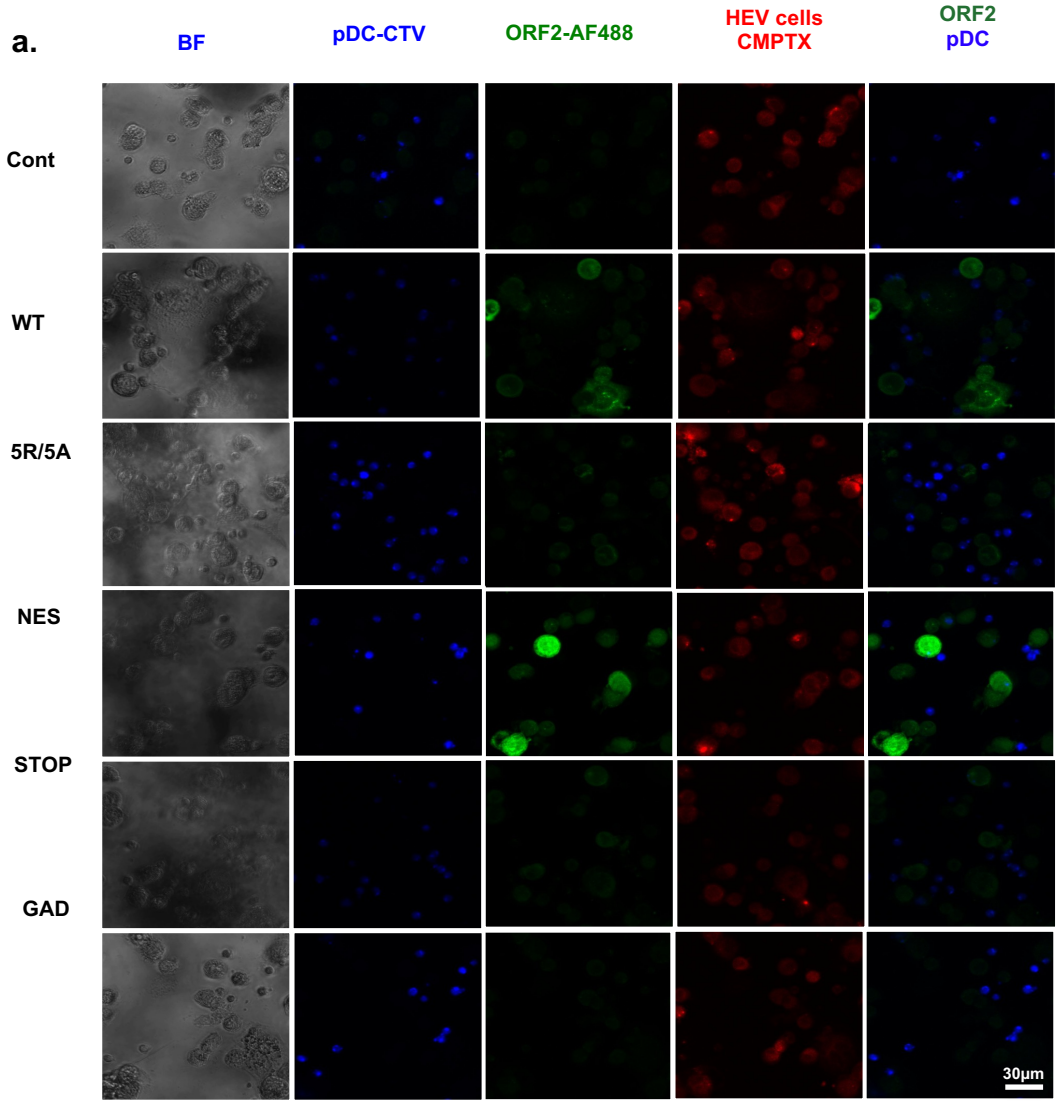
a.
BF
pDC-CTV
ORF2-AF488
HEV cells
CMPTX
ORF2
pDC
Cont
WT
5R/5A
NES
STOP
GAD
30µm

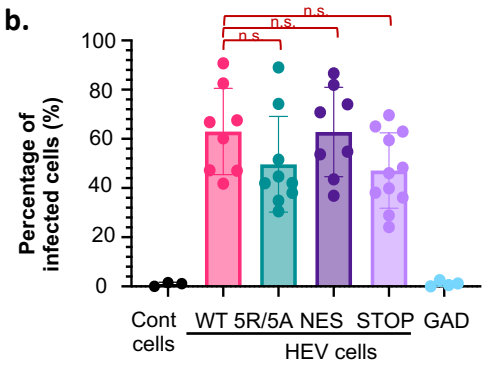
b.
Percentage of infected cells (%)
100
80
60
40
20
0
n.s.
n.s.
n.s.
Cont cells
WT
5R/5A
NES
STOP
GAD
HEV cells

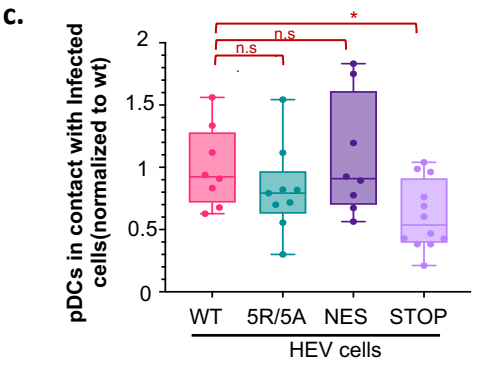
c.
pDCs in contact with Infected cells(normalized to wt)
2
1.5
1
0.5
0
n.s
n.s
*
WT
5R/5A
NES
STOP
HEV cells

Figure 4